

EFFECT OF SILVER NANOPARTICLES ON TOMATO PLANTS AND
DEVELOPMENT OF A PLANT MONITORING SYSTEM (PMS)

LeVar Marquel Odum

A Thesis

Submitted to

the Graduate Faculty of

Auburn University

in Partial Fulfillment of the

Requirements for the

Degree of

Master of Science

Auburn, Alabama
December 17, 2007

EFFECT OF SILVER NANOPARTICLES ON TOMATO PLANTS AND
DEVELOPMENT OF A PLANT MONITORING SYSTEM (PMS)

Except where reference is made to the work of others, the work described in this thesis is my own or was done in collaboration with my advisory committee. This thesis does not include proprietary or classified information.

LeVar Marquel Odum

Certificate of Approval:

Aleksandr Simonian
Professor
Materials Engineering

ZhongYang Cheng, Chair
Associate Professor
Materials Engineering

Bryan A. Chin
Department Chair/ Professor
Materials Engineering

Bart Prorok
Associate Professor
Materials Engineering

George T. Flowers
Interim Dean
Graduate School

EFFECT OF SILVER NANOPARTICLES ON TOMATO PLANTS AND
DEVELOPMENT OF A PLANT MONITORING SYSTEM (PMS)

LeVar Marquel Odum

Permission is granted to Auburn University to make copies of this thesis at its discretion,
upon request of individuals or institutions and at their expense. The author reserves all
publication rights.

Signature of Author

Date of Graduation

VITA

LeVar Marquel Odum, son of Tommy and Magdalene Odum, was born on July 25th, 1977, in Tuscaloosa, Alabama. He attended the University of Alabama at Birmingham in September 1997 and graduated with a Bachelor of Science in Electrical Engineering in June 2001. In 2005, he entered Graduate School at Auburn University to pursue a Masters degree in Materials Engineering.

THESIS ABSTRACT

EFFECT OF SILVER NANOPARTICLES ON TOMATO PLANTS AND DEVELOPMENT OF A PLANT MONITORING SYSTEM (PMS)

LeVar Marquel Odum

Master of Science, December 17, 2007
(B.S.E.E, University of Alabama at Birmingham, Birmingham, 2001)

76 Typed Pages

Directed by Zhong Yang Cheng

Smart Agriculture will determine whether farmers in the US can compete internationally. Engineering plays a significant role in Smart Agriculture through the development of sensor networks, data acquisition, and control systems that will help advance the fundamental understanding of food quality and plant growth. In this thesis, two issues related to engineering in Smart Agriculture are studied: 1) the influence of nano-materials on plants; and 2) the development of a plant monitoring system.

The influence of silver (Ag) nanoparticles on tomato plant growth is studied. Silver nanoparticles have become a significant tool in the development of novel biological and chemical processes. Silver nanoparticles have unique physical and chemical properties, such as the ability to kill or impede growth of bacteria and

microorganisms such as *E. coli*. With the growth of silver nanoparticles usage, it is only a matter of time before silver nanoparticles are heavily distributed into the ecosystem. For that reason, it is critical to study the long-term effects of silver nanoparticles on our food supply, such as plants and crops.

In this study, tomato plants are grown hydroponically, in solution with known concentrations (1.97×10^{13} and 1.57×10^{11}) of silver nanoparticles. Silver nanoparticles ranging in sizes from 10 nm to 50 nm were investigated. The uptake or absorption of the silver nanoparticles by the tomato plants was monitored using a Ultra-Violet/vis Spectrophotometer. Material characterization technologies, such as X-ray Diffraction, Raman Spectroscopy, and Energy Dispersive Spectrometer were then used to determine the location of the silver nanoparticles in the plants. The growth of plants was visually observed and recorded. Based on experimental results, it was concluded that tomato plants uptake the silver nanoparticles from the hydroponic solution and these silver nanoparticles led to the death of the plants. It was also found that the smaller the silver nanoparticles, the quicker the tomato plants die.

This thesis also investigated the use of sensors, data acquisition systems, and wireless networks to monitor the growth and health of plants. A plant monitoring system was designed and fabricated to monitor plants. This system was designed to operate over a wide temperature range, have low-power consumption, and be robust in nature. A multitude of sensors was wired to the data acquisition system. Bluetooth, the wireless protocol of choice, was then used to communicate the information from the data acquisition system to a remote computer monitoring station. The system monitored and recorded temperature, humidity, soil moisture, and ripeness of fruit and/or vegetables.

ACKNOWLEDGEMENTS

The author would like to express his sincere thanks and gratitude to his major professor, Dr. ZhongYang Cheng, for his guidance and support during his graduate studies. He would also like to thank Dr. Bryan Chin for his advice and guidance through his graduate degree. Thanks are also due to Dr. Aleksandr Simonian for his helpful suggestions. Thanks are due to Joseph Wu for his help in nanoparticles synthesis.

The author would also like to thank Dr. Bart Prorok for all his advice and suggestions during his research. Appreciation is due to Dr. Clyde Wickle, L.C. Mathison, Antoine Harvis, and Shirley Lyles for all their help.

The author would also like to thank his wife (Nicole), his parents and his siblings for their love and support.

Style manual or journal used: Auburn University Guide To Preparation
And Submission Of Thesis And Dissertations

Computer software used: Microsoft Word XP, Microsoft Excel, Orcad
Capture, Orcad Layout, Origin

TABLE OF CONTENTS

LIST OF FIGURES	xi
LIST OF TABLES	xiv
1. EFFECT OF SILVER NANOPARTICLES	1
1 Properties of Silver Nanoparticles	1
1.1.1 Physical Characteristics	1
1.1.2 Toxic Effects of Silver Nanoparticles.....	3
1.2 Phytoremediation versus Nanoparticle Uptake.....	4
2. OBJECTIVES OF RESEARCH.....	7
3. SYNTHESIS OF SILVER NANOPARTICLES	8
4. EXPERIMENTS	11
4.1 Detection of silver nanoparticles	11
4.1.1 X-ray Diffraction (XRD)	11
4.1.2 Energy Dispersive Spectrometer (EDS)	15
4.1.3 Raman Spectroscopy.....	16
4.1.4 Ultra-Violet Spectrophotometer (UVS).....	19
4.2 UVS Sample Preparation	20
4.2.1 Citrate/Borohydride Control Test	23

5. RESULTS AND DISCUSSIONS.....	25
5.1 Experimental Results	25
5.2 Conclusions.....	32
6. FUTURE WORK.....	34
7. PLANT MONITORING SYSTEM	35
8. OBJECTIVES OF RESEARCH.....	37
9. CIRCUIT DESIGN.....	38
9.1 Microcontroller Selection	39
9.2 Wireless Communication Selection.....	40
9.3 Board Layout	45
9.4 Software	49
10. SENSING NETWORK.....	51
11. EXPERIMENTS	52
11.1 Set-up	52
12. RESULTS AND DISCUSSIONS.....	56
12.1 Conclusion	59
13. FUTURE WORK.....	60
BIBLIOGRAPHY	61

LIST OF FIGURES

Fig.1.1.1	Logarithmic plot of spherical particle radius versus surface area-to-volume ratio.....	2
Fig. 1.1.1.2	Diagram illustrating Ag particles sizes versus active sites for microorganism attachment.....	3
Fig.1.1.2.1	TEM images of <i>P. aeruginos</i> samples.....	4
Fig.1.1.2.2	Diagram of phytoremediation versus nanoparticle uptake illustration.....	6
Fig.3.1	SEM image of 50 nm Ag nanoparticles.....	9
Fig.3.2	a) TEM image of 50 nm Ag nanoparticles and b) TEM image of 10 nm Ag nanoparticles	10
Fig. 4.1.1.1	Schematic of a typical XRD powder diffraction (Siemens manual)	12
Fig. 4.1.1.2	XRD plots of the first 2 θ peaks for a) 10 nm and b) 50 nm sized silver nanoparticles	12
Fig. 4.1.1.3	Tomato plants after two weeks for XRD.....	14
Fig. 4.1.1.4	The XRD plots for the tomato plants roots (10 nm and 50 nm).....	14
Fig. 4.1.3.1	Schematic of Raman Spectroscopy	16
Fig. 4.1.3.2	Raman spectra for citrate synthesized silver nanoparticles	17
Fig. 4.1.3.3	Raman spectra for leaves (top) and stems (bottom) of tomato plants	18
Fig. 4.1.4.1	UVS/vis operation schematic diagram	19

Fig. 4.2.1	a) Tomato plant in a cuvette filled with 1 mL of citrate solution of 50 nm silver nanoparticles and b) Tomato plant in a cuvette filled with 1 mL of borohydride solution of 10 nm silver nanoparticles	21
Fig.4.2.1.1	Schematic of citrate/borohydride control test.....	23
Fig. 4.2.1.2	a) UVS Spectra of pure citrate solution b) UVS Spectra of pure borohydride solution	24
Fig. 4.2.1.3	a) UVS spectra of 50 nm silver particles in plant immersed citrate solution using the sequence shown in Figure 4.2.1.1. b) UVS spectra of 10 nm silver particles in plant immersed borohydride solution using the sequence shown in Figure 4.2.1.1.....	24
Fig. 5.1.1	Cycle 1, UVS spectra of tomato plant samples in 10 nm and 50 nm Ag nanoparticles solutions and reference solutions.....	26
Fig. 5.1.2	Cycle 2, UVS spectra of tomato plant samples in 10 nm and 50 nm Ag nanoparticles solutions and reference solutions.....	27
Fig. 5.1.3	Cycle 3, UVS spectra of tomato plant samples in 10 nm and 50 nm Ag nanoparticles solutions and reference solutions.....	28
Fig. 5.1.4	Cycle 4, UVS spectra of tomato plant samples in 10 nm and 50 nm Ag nanoparticles solutions and reference solutions.....	29
Fig. 5.1.5	Cycle 5, UVS spectra of tomato plant samples in 10 nm and 50 nm Ag nanoparticles solutions and reference solutions.....	30
Fig. 5.1.6	Image of samples and reference	31
Fig. 5.1.7	Raman spectra of leaves after UVS cycle 5 with 0.1% power of 514 nm light source.....	32
Fig. 5.2.1.	Slopes of 10nm Ag nanoparticles uptake in tomato	33
Fig. 5.2.2.	Slopes of 50nm Ag nanoparticles uptake in tomato	33

Fig. 7.1	Illustration of the concept of smart agriculture with wireless communication.....	36
Fig. 9.1	Block diagram of PMS	38
Fig. 9.2.1	Comparison of the different wireless protocols.....	43
Fig. 9.2.2	Bluetooth Module.....	43
Fig. 9.3.1	PMS prototype board.....	46
Fig. 9.3.2	PMS circuit board schematic drawing.....	47
Fig. 9.4.1	PMS C-programming flow-diagram.....	50
Fig. 11.1.1	Experiment Setup for PMS testing	53
Fig. 11.1.2	Screen print of HyperTerminal capturing PMS output data.....	54
Fig. 11.1.3	Environmental chamber used for temperature test.....	55
Fig. 12.1	Graph of PMS soil readings.....	58

LIST OF TABLES

Table 3.1	Size and concentration of silver nanoparticles solutions	10
Table 4.1.2.1	EDS scans on the leave, stem, and root of tomato plant in 10 nm nano-silver.....	15
Table 4.2.1	Refills performed in experiment.....	22
Table 9.1.1	List of selected low power microcontrollers.....	40
Table 9.2.1	List of wireless technology modules and their parameters.....	44
Table 9.3.1	PMS power consumption.....	46
Table 9.3.2	PMS Bill of materials	48
Table 12.1	Temperature and humidity data recorded (PMS and reference).....	57
Table 12.2	Results of temperature extreme operation test.....	58

1. EFFECT OF SILVER NANOPARTICLES

1.1 Properties of Silver Nanoparticles

Nanoparticles are utilized in cosmetic, medical and military applications due to their unique chemical and physical properties. The unique properties of these nanomaterials are highly dependent upon their size and shape. Nanometer sized particles tend to exhibit very different properties than their bulk scaled counterparts. The small size of the silver nanoparticles is reported to improve the antibacterial properties of silver in addition to improving chemical durability (Toshikazu, 1999). The antibacterial properties of silver nanoparticles have led to several new products such as nanoparticles embedded clothes dryers sheets to reduce clothing (socks) odors and antibacterial soap and toothpaste.

1.1.1 Physical Characteristics

For silver nanoparticles, the enhanced properties are due to the large surface area-to-volume ratio. This larger ratio significantly increases the antibacterial effects by allowing easier interaction with other particles (Lee et al., 2004).

The volume, V , of spherical particles is defined as:

$$V = \frac{4}{3} \pi r^3 \quad (1.1)$$

and the surface area, SA, is given by:

$$SA = 4 \pi r^2 \quad (1.2)$$

where r is the particle's radius.

Therefore, the surface area-to-volume ratio is given by:

$$(SA/V) = 3/r \quad (1.3)$$

From this equation it is evident that the surface area-to-volume ratio is inversely proportional to the particle radius. Figure 1.1.1.1 plots this relationship. As the particle size decreases, the number of active surface sites increases, relative to inactive, internal sites, enhancing the material properties. The larger particle internal active sites are not exposed to forces or reactions, reducing the particles material properties. Figure 1.1.1.2 displays a diagram illustrating particles' size versus active sites for microorganism interaction.

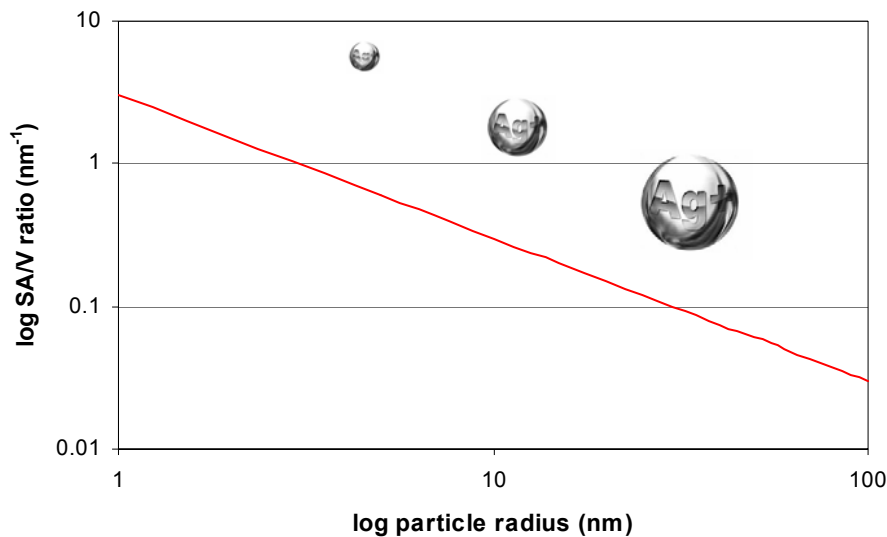


Figure 1.1.1.1. Logarithmic plot of spherical particle radius versus surface area-to-volume ratio

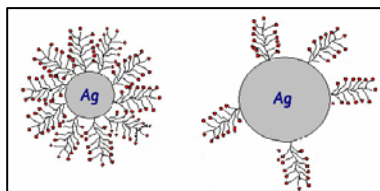


Figure 1.1.1.2. Diagram illustrating Ag particles size versus active sites for microorganism attachment

1.1.2 Toxic Effects of Silver Nanoparticles

It has been well known for thousands of years that silver ions and silver-based compounds are highly toxic toward many microorganisms and have shown fatal effects to many of bacteria (Sondi and Sondi, 2004). Recent studies have also demonstrated silver nanoparticles' ability to attach to human immunodeficiency virus (HIV-1), hindering the virus' ability to bind to the host cells (Elechiguerra et al., 2005).

The exact mechanism by which silver nanoparticles destroy and prevent pathogen growth is not well understood. There are many possible mechanisms discussed by researchers but the exact mechanism has not been confirmed. One researcher states that in order to understand the antibacterial mechanism of silver nanoparticles, one has to first understand how bacteria and viruses live and grow. Bacteria are believed to use an enzyme to metabolize oxygen to sustain life. Silver ions cripple the enzyme and stop the metabolization of oxygen. This suffocates the bacteria, resulting in its death. Viruses grow by invading living cells and then reproducing replicas of itself. As part of the process, the cell relies upon oxygen metabolizing enzymes. Again, silver ions kill the virus-producing cell by suffocation (Puebla et al., 2004). Another study suggests that monovalent silver ions (Ag^+) replace hydrogen cations (H^+) of sulfhydryl or thiol (S-H) groups on the surface of cellular membranes. This disables the production of proteins

require to sustain the cell, resulting in eventual death of the cell (Feng and Wu et al., 2000). However, one study shows that not only the surface of the cell is affected but the inside of the cell is also exposed to the effects of the silver nanoparticles (Morones et al., 2005). Figure 1.1.2.1 shows (a) Control cells of *P. aeruginosa* and (b) Cells of *P. aeruginosa* disrupted by silver nanoparticles.

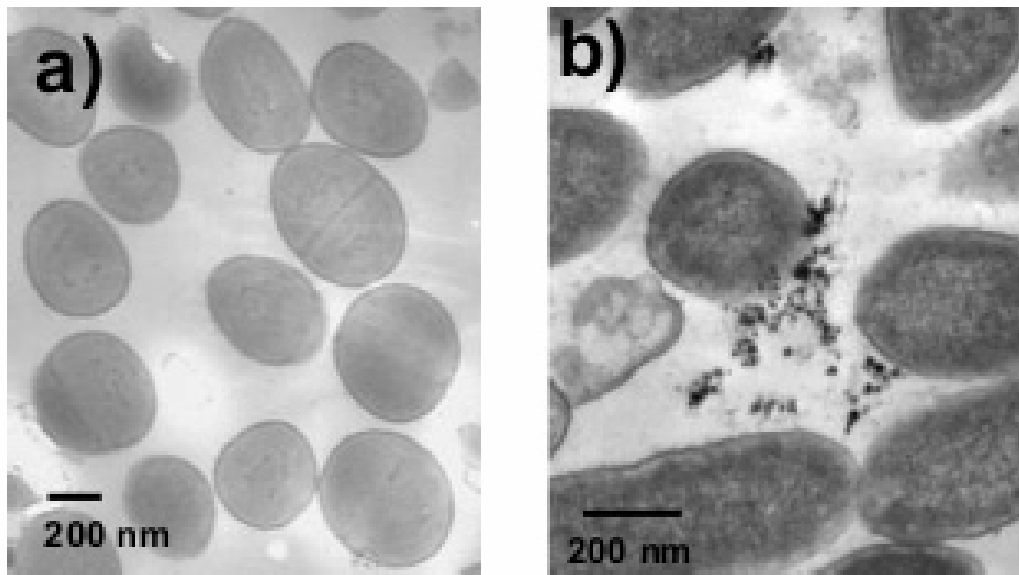


Figure 1.1.2.1. TEM images of *P. aeruginos* samples. (Morones et al., 2005)

Figure 1.1.2.1 (b) shows silver nanoparticles on the surface as well as inside the *P. aeruginosa* cells.

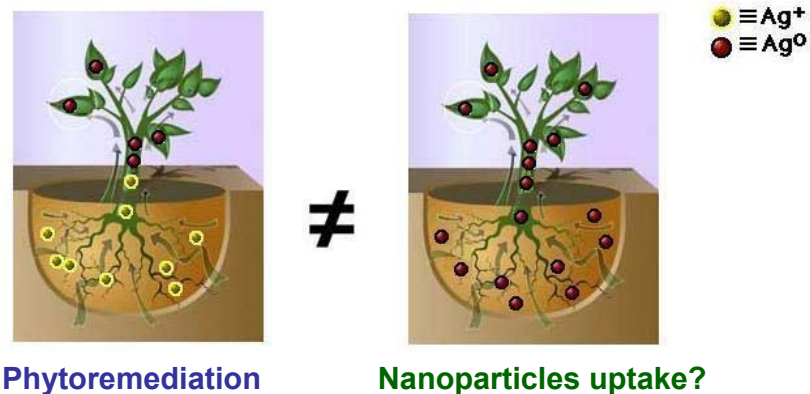
Despite the uncertainty of the exact mechanism of interaction, and that very little is known regarding the effects of silver nanoparticles on the environment and human health, silver nanoparticles are still being widely used because of their toxicity toward microorganisms.

1.2 Phytoremediation versus Nanoparticle Uptake

Contaminated soil and water poses a great threat to vegetation and a dangerous health risk for people around the world. Heavy metals ions at high concentrations are one of the most harmful contaminants, however, they are ubiquitous on earth. At normal concentrations (less than 1000 parts per million (ppm)) most heavy metal ions are harmless to living organisms (Gardea-Torresdey et al., 2005).

Although there are several current technologies that can be used for cleaning sites contaminated with heavy metals, they tend to be expensive and labor intensive. Natural remediation by plants has recently become a possible alternative. One of the promising alternative methods, phytoremediation uses plants to purify the water and soil contaminated with heavy metal ions, such as silver. During phytoremediation, metallic ions are absorbed by plants. Accumulation of these ions eventually leads to the synthesis/formation of metal nanoparticles inside the plant's tissues (Gleba et al., 1999). However, to the best of our knowledge, the mechanism by which the plants absorb nanoparticles of silver is not well known. The possible effects of silver nanoparticle contamination of food, such as vegetables, must be studied since vegetation may uptake nanoparticles from contaminated soil and water.

In phytoremediation, the synthesis of metal nanoparticles in plant tissue results in very high concentrations of the nanoparticles in the plant (Gardea-Torresdey et al., 2005). However, if previously formed nanoparticles are absorbed by a plant, it is assumed that the tissue will have a lower concentration of nanoparticles. Figure 1.1.2.2 illustrates the differences between phytoremediation and nanoparticle absorption. In Figure 1.1.2.2, Ag^+ symbolizes the silver ions and Ag^0 symbolizes the synthesized silver nanoparticles.



High Concentration of Ag⁰

Low Concentration of Ag⁰

Figure 1.1.2.2. Diagram of phytoremediation versus nanoparticle uptake illustration (http://polaris.umuc.edu/cvu/envm/phyto/html/org_Ia.jpg)

A few studies describing the effects of nanoparticles on living plants were found in the literatures. One study found that alumina nanoparticles impeded the growth of seed roots of five plant species (corn, cucumber, soybean, cabbage, and carrot) (Yang and Watts, 2005). Another study using nanoparticles of carbon tubes, zinc, zinc oxide, alumina and aluminum was conducted on the root growth of seeds of radish, rape, ryegrass, lettuce, corn, and cucumber (Lin and Xing, 2007). This study concluded that the nanoparticles impeded the growth of the seed resulting in shorter root elongation compared to a control group. The study also found that if the seeds were fed smaller size nanoparticles, the root elongations measured were even shorter than seeds fed larger nanoparticles. No studies were found that describe the mechanism by which silver nanoparticles affect the uptake, translocation and growth of plants.

2. OBJECTIVES OF RESEARCH

Silver nanoparticles have recently been heavily used in cosmetic and medical products which have raised growing concerns about the environmental effect that these nanoparticles may have on the vegetation since it is well known that silver is highly toxic to microorganisms. The objectives of this thesis were:

- To determine whether silver nanoparticles can be absorbed by tomato plants.
- If silver nanoparticles are absorbed, where in the plant do the silver nanoparticles accumulate?
- To observe the effect of the silver nanoparticles on the growth of tomato plants.

3. SYNTHESIS OF SILVER NANOPARTICLES

Silver nanoparticles can be synthesized using several different techniques such as chemical reduction, laser ablation, photochemical and electrochemical methods. The most popular method is chemical reduction of silver nitrate (AgNO_3) using sodium citrate ($\text{C}_6\text{H}_5\text{O}_7\text{Na}_3$) or sodium borohydride (NaBH_4). The preparation is simple, but requires care and cleanliness (Sileikaite et al., 2006). In this research, spherical silver nanoparticles were prepared using both borohydride and citrate reduction of silver nitrate.

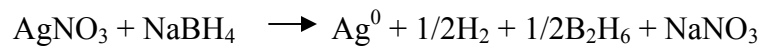
The 50 nm particles were prepared according to (Lee and Meisel, 1982). 16.9 mg (1 mM) of silver nitrate was dissolved in 100 mL of distilled water. The solution was heated to a boil using a heating plate while the solution was vigorously agitated with a magnetic stirrer. After 2 minutes of boiling, 2 mL of 1% trisodium citrate was rapidly added. The solution turned a grayish color within a few minutes, indicating the synthesis of Ag nanoparticles. The solution was kept boiling for 10 minutes, which determined the size of nanoparticles, by allowing more chemical reduction time. The solution was then removed from the heating plate and allowed to cool.

The reaction that occurred to form the 50nm silver nanoparticles is as follows:



The 10 nm Ag nanoparticles were prepared using borohydride reduction method. In 100 ml of deionized water, 16.9 mg (1 mM) of silver nitrate was dissolved and the solution was kept in ice bath for half an hour. The ice cold silver nitrate solution was added slowly to 300 mL of vigorously stirred ice-cold (2 mM) NaBH₄. A yellow Ag particle solution was obtained.

The reaction that occurred to form the 10nm silver nanoparticles is as follows:



Shape and size of the silver nanoparticles were analyzed with scanning electron microscopy (SEM) and transmission electron microscopy (TEM). Typical images of the silver nanoparticles are shown in Figure 3.1 and Figure 3.2.



Figure 3.1. SEM image of 50 nm Ag nanoparticles

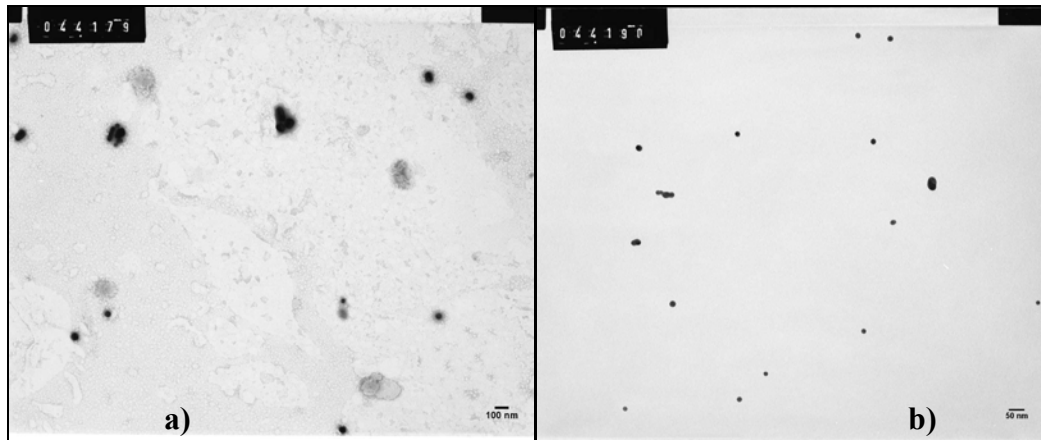


Figure 3.2. a) TEM image of 50 nm Ag nanoparticles; b) TEM image of 10 nm Ag nanoparticles

The concentration of the silver nanoparticle solutions was calculated, assuming all silver atoms were reacted and became particles. The atomic radius and density of Ag is 1.6×10^{-8} cm and 10.5 g/cm^3 , respectively. The atomic mass of Ag, A.M., was calculated by multiplying the volume (eq. 1.1) and the density. By replacing the atomic radius with the particle radius measured through SEM and TEM investigations, the particle mass, P.M., was also obtained. Dividing P.M. by A.M provided the number of Ag ions per particle, $N_{\text{ion-particle}}$. The number of Ag ions in 1 mM of solution, $N_{\text{ion-solution}}$, was calculated by multiplying the number of moles, the number of grams, and Avogadro's number. Therefore, the number of Ag particles per mL, $N_{\text{particles/mL}}$, was determined by

$$N_{\text{particles/mL}} = [N_{\text{ion-solution}} / N_{\text{ion-particle}}] * (1/ 100 \text{ mL}). \quad (3.1)$$

A list of the size and concentration of the silver nanoparticle solutions is given in Table 3.1 below.

Particle Size (nm)	# of Particle per mL
50	1.57E+11
10	1.97E+13

Table 3.1. Size and concentration of silver nanoparticle solutions

4. EXPERIMENTS

4.1 Detection of silver nanoparticles

The presence of the silver nanoparticles in tomato plants must be detected so that uptake can be determined. There are many methods for detecting silver nanoparticles, but the detection in plant tissue requires specialized sample preparation. Most preparation methods involve harsh chemical treatment or high temperature ashing of the tissue. In an attempt to avoid lengthy preparation procedures for plant tissue analysis, XRD was attempted based on previous research literature where X-ray diffraction was used in a similar way to confirm formation of silver nanoparticles in white rot fungus (Vigneshwaran et al., 2006). Energy Dispersive Spectrometry (EDS), Raman Spectroscopy and UV/vis Spectrophotometry were also used.

4.1.1 X-ray Diffraction (XRD)

XRD is commonly used for determining the chemical composition and crystal structure of a material; therefore, detecting the presence of silver nanoparticles in plants tissues can be achieved by using XRD to examine the diffraction peaks of the plant. In Figure 4.1.1.1 a typical schematic of a XRD powder diffractometer is illustrated.

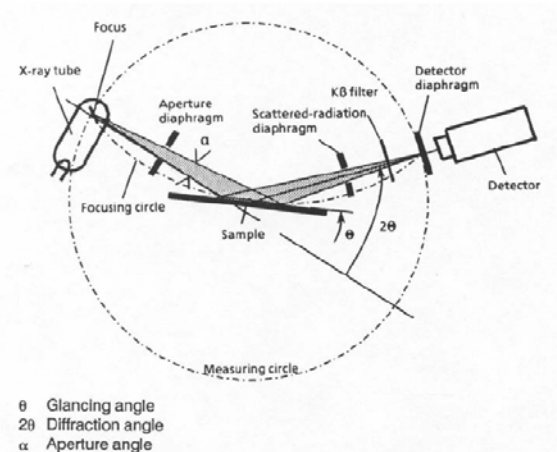


Figure 4.1.1.1. Schematic of a typical XRD powder diffractometer (Siemens manual)

In order to detect the silver nanoparticles in plant tissues, the diffraction patterns of silver must be established first. This is done by performing XRD on the silver nanoparticles themselves. Using Bragg's Law, the (111) peak was calculated. The silver nanoparticles particles were found to be amorphous and had to be crystallized before using XRD. The silver nanoparticles were prepared for XRD by pipetting a small amount of well-mixed particle solution on a silicon wafer and then heat treated in an Argon atmosphere at 400 °C for 1.5 hr. to crystallize the particles. Figure 4.1.1.2 shows the XRD plots of the first 2θ peaks of 10 nm and 50 nm sized silver nanoparticles.

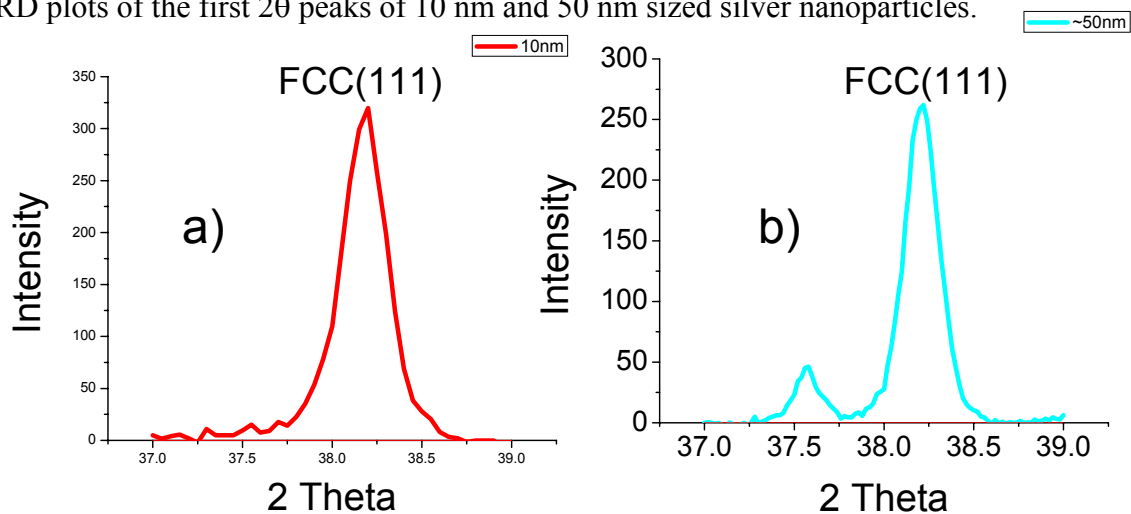


Figure 4.1.1.2. XRD plots of the first 2θ peaks for a) 10 nm and b) 50 nm sized silver nanoparticles.

The first 2θ peak, the (111) peak, is focused on because it has the smallest diffraction angle which tends to produce the greatest peak amplitude and is more likely to penetrate the plant tissue. Peaks for both particles sizes were in agreement with the 2θ peak value of 38.25° for the first 2θ peak for silver in the Joint Committee on Powder Diffraction Standards (JCPDS). From the peaks, the expected size of the particles was estimated as ~ 6.5 nm and ~ 53.4 nm using the Debye Scherrer equation seen below:

$$D = 0.9 \lambda / \beta \cos \theta \quad (4.1)$$

where λ – wavelength of radiation, β - FWHM (Full width at half maximum), and θ - the angle of the maximum of diffraction. It is critical to note that the Debye Scherrer equation has size limitations causing errors in size estimation for particles less than 20 nm. In addition, there may be errors due to particle distribution within the sample.

Preparation of tomato plants for XRD was as follows:

For two weeks, two tomato plants were introduced to 10 nm and 50 nm sized silver nanoparticles, each at a low concentration of 10^4 particles in 16 ml of nutrient solution. A reference plant without exposure to silver nanoparticles was used as a control. The leaves, stems, and roots were cut off and analyzed for silver particle uptake. A picture of the plants after two weeks is shown in Figure 4.1.1.3. The plant samples were then heat treated in an Argon atmosphere at 400°C for 1.5 hour to crystallize the particles and to burn away the organic tissues. Upon XRD analysis, there were no diffraction peaks visible in the leaves, stems and roots. Figure 4.1.1.4 shows the absence of the diffraction peaks in the XRD plots for the roots of the tomato plants. The absence of the peaks could

be due to the low concentration of silver nanoparticles absorbed. Therefore, XRD is not sensitive enough to detect the low concentration of silver nanoparticles in plant tissue.

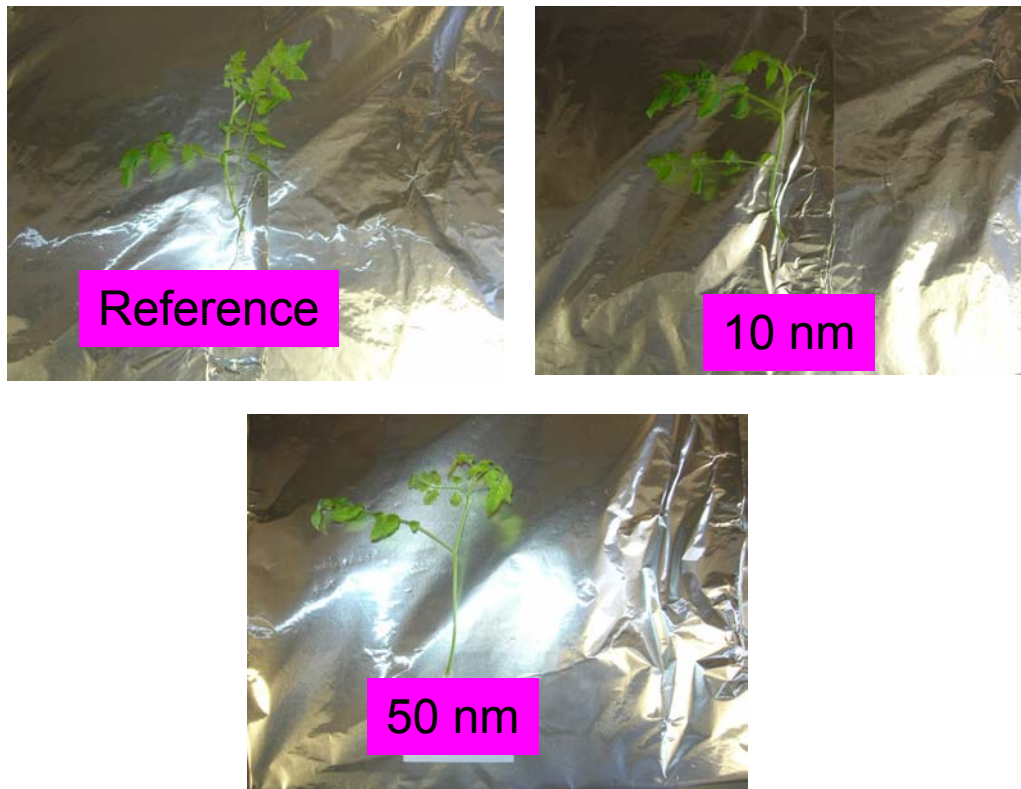


Figure 4.1.1.3. Tomato plants after two weeks for XRD

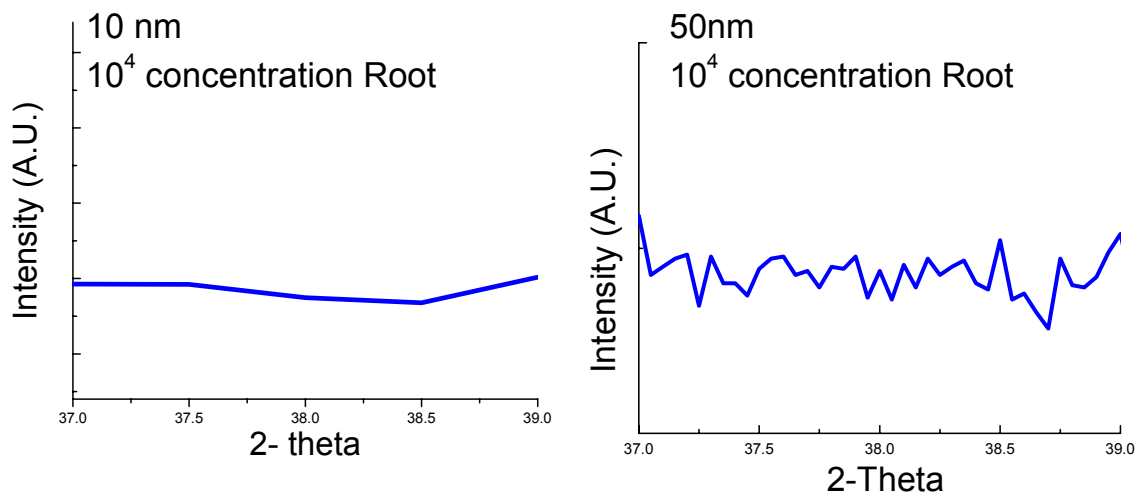


Figure 4.1.1.4. The XRD plots for the tomato plants root (10 nm and 50 nm)

4.1.2 Energy Dispersive Spectrometry (EDS)

Energy Dispersive Spectrometry (EDS) micro-analysis is performed by measuring the energy and intensity distribution of X-ray signals generated by a focused electron beam on a specimen. The data is used to obtain the elemental composition of the material. This method is a good candidate for identifying silver in the tissue of tomato plants.

The plants prepared for XRD analysis were also used for this analysis. It is assumed that the 10 nm silver nanoparticles are more likely to be absorbed in the plant at higher concentrations than the 50 nm silver nanoparticles. The leaf, stem and root of the plant fed 10 nm particles were used in this analysis. The results of the EDS scans are shown in Table 4.1.2.1 below.

Element	keV	Wt%	At%	Element	keV	Wt%	At%	Element	keV	Wt%	At%
Na	1.041	0.26	0.44	P	2.013	10.02	12.18	Na	1.041	0.30	0.50
P	2.013	2.96	3.68	Cl	2.622	14.10	14.97	P	2.013	11.62	14.47
Cl	2.622	18.26	19.84	K	3.313	68.00	65.46	Cl	2.622	6.60	7.18
K	3.313	72.01	70.94	Ca	3.691	7.87	7.39	K	3.313	49.54	48.84
Ca	3.691	4.33	4.16	Ag	2.984	0.00	0.00	Ca	3.691	28.76	27.66
Y	1.922	2.18	0.95	Na	1.041	0.00	0.00	Y	1.922	2.75	1.19
Ag	2.984	0.00	0.00	Y	1.922	0.00	0.00	Ag	2.984	0.42	0.15
Total		100.00	100.00	Total		100.00	100.00	Total		100.00	100.00

Leaf

Stem

Root

Table 4.1.2.1. EDS scans on the leaf, stem and root of tomato plant in 10nm nano-silver

The EDS output showed very little to no silver in the atomic percentage of the elemental composition of the plant. The data showed a small amount of silver in the root; however, the concentration of silver nanoparticles in the root is lower than the detection limit of the EDS system, which means the test is inconclusive.

4.1.3 Raman Spectroscopy

In Raman Spectroscopy, light is scattered inelastically from molecules providing information about the molecules' vibrational quantum states. The scattered signal is rather weak, but can be greatly strengthened if the molecules are attached to metal nanoparticles. A schematic of Raman Spectroscopy operation can be seen in Figure 4.1.3.1 below.

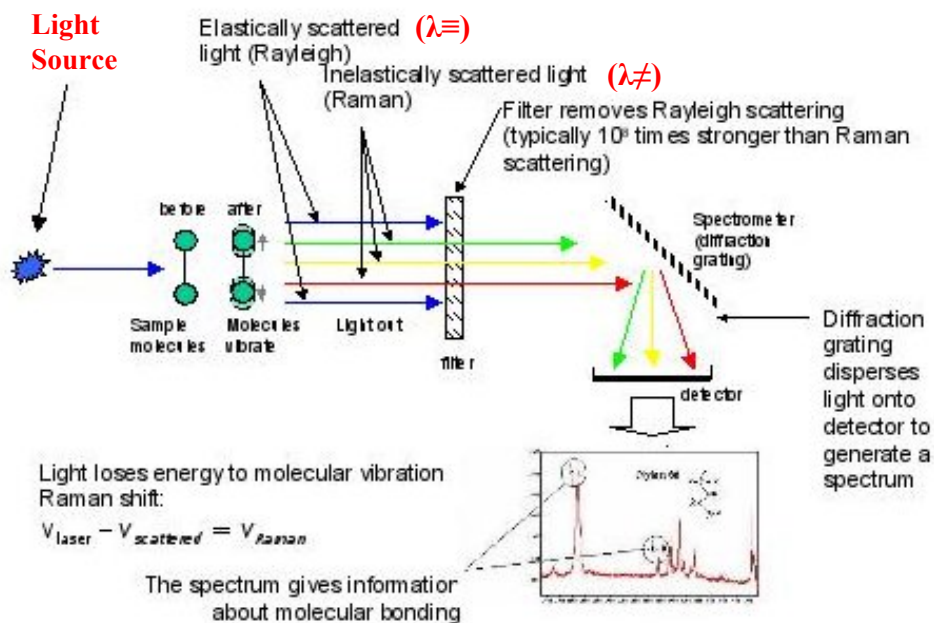


Figure 4.1.3.1 Schematic of Raman Spectroscopy
(<http://newton.ex.ac.uk/research/biomedical/optics/sers.html>)

Silver nanoparticles are a common material used in Raman Spectroscopy and data of their Raman scattering are widely documented. In Figure 4.1.3.2, a plot of Raman spectra for synthesized silver nanoparticles is displayed. This plot was used as a reference for the silver nanoparticles peaks in this research.

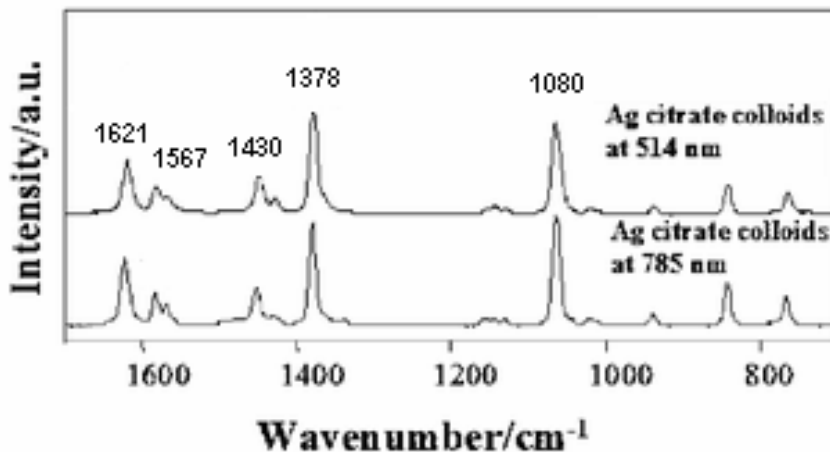
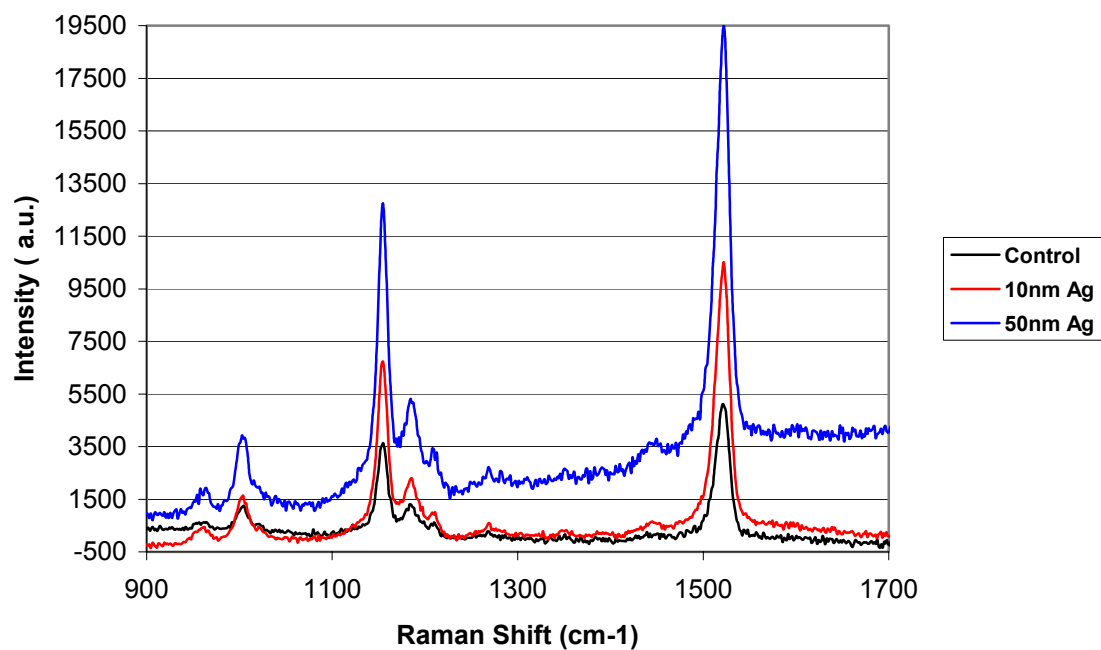


Figure 4.1.3.2. Raman spectra for citrate synthesized silver nanoparticles (Puebla et al.,2004)

Two tomato plants were exposed to silver nanoparticles, 10 nm and 50 nm in size respectively. Both had a concentration of 10^{11} particles in 16 ml of nutrients solution for two days. A reference plant without exposure to silver nanoparticles and the two plants exposed to silver nanoparticles were cut and separated into leaves, stems and roots for analysis. The Raman spectra of the leaves and stems of the plants are shown in Figure 4.1.3.3. The roots were not used because they were too small to analyze with this method.

Raman spectra of tomato plant (Leaves)



Raman Spectra of tomato plant (Stems)

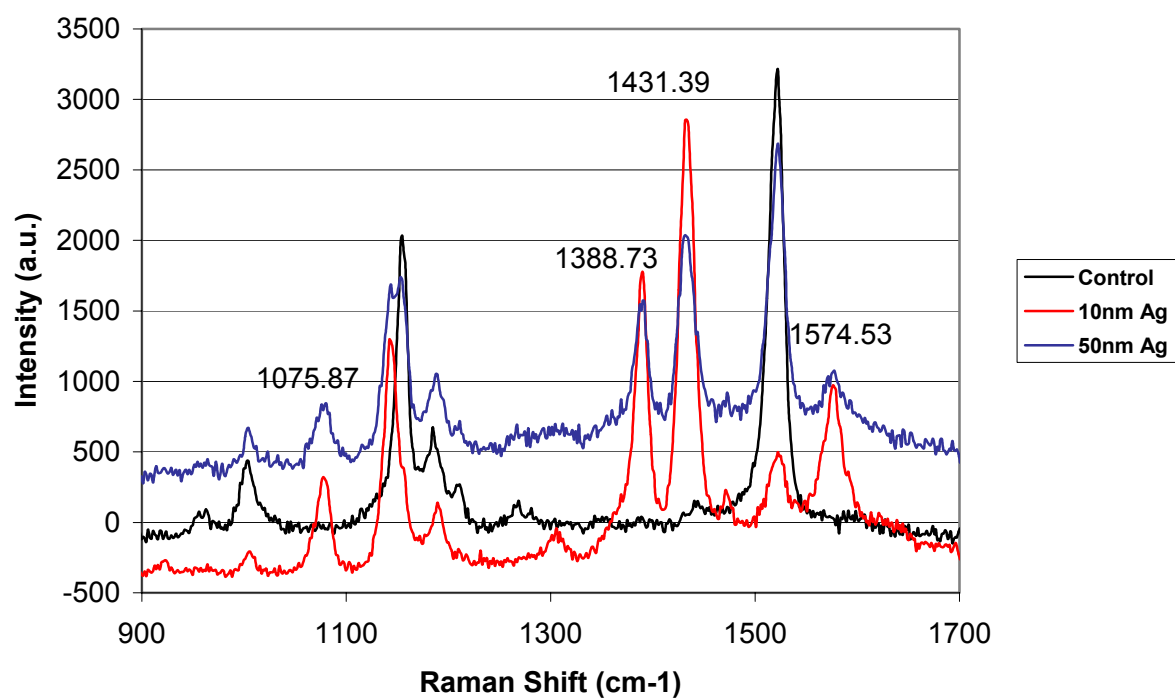


Figure 4.1.3.3. Raman spectra for leaves (top) and stems (bottom) of tomato plants

From the Raman spectra shown in Figure 4.1.3.3, the stems of the plants had several more spectrum than the control plant. These extra peaks are in good agreement with the peaks seen in Figure 4.1.3.2, which confirms that the peaks are from silver nanoparticles. The spectra from the leaves of the tested plant are not much different from the control plant. Therefore, silver nanoparticles were absorbed in the plant through the roots and within the stem but not to the leaves within the two days. Raman Spectroscopy proved to be an effective method in determining the uptake of silver nanoparticles in plants.

4.1.4 UV/vis Spectrophotometry (UVS)

UV/vis Spectrophotometry (UVS) is a technique for characterizing and measuring the absorbance of a species in solution by passing white light through a cuvette containing the sample. The intensity of the transmitted beam at different wavelengths is related to the concentration of the species in solution. Figure 4.1.4.1 below is a schematic illustration of UVS operation. The absorbance spectrum between 400 nm to 450 nm is known to be for spherical silver nanoparticles (Sileikaite, et al., 2006).

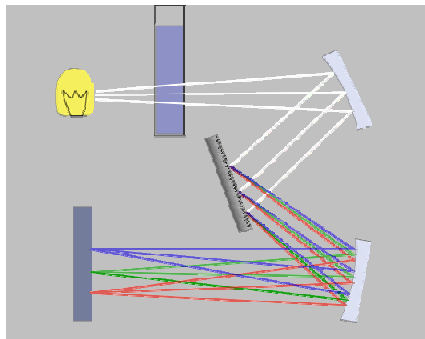


Figure 4.1.4.1. UVS operation schematic diagram (<http://en.wikipedia.org/wiki/Image:UV-vis.png>)

The equipment used in this test was a computer-controlled Ultrospec 2100 pro spectrophotometer using the SWIFT II software. It is well known that the absorption (A) of light by the solution is dependent on three parameters: the extinction coefficient (ϵ), the concentration (c), and the path length (L) as described by Beer-Lambert Law as

$$A = \epsilon * c * L \quad (4.2)$$

For the instrument used in this study, $L = 1$ cm. For a certain solution placed in a fixed cuvette, equation 4.2 indicates that the absorption is proportional to the concentration of the solution. If the reduction in the intensity of the transmission beam is due to the reduction of the concentration of the solution, then the transmission beam can be utilized to determine the plant absorption of the silver nanoparticles by determining the concentration using equation 4.2.

4.2 UVS Sample Preparation

The Supersweet 100, Hybrid tomato seeds were obtained and grown hydroponically. After two weeks the plants were big enough so that stems with leaves about 3" long were cut from the plants as test samples, which were then immediately planted in cuvettes used for spectrophotometry. Each cuvette, the top of which was punctured with a small hole, was filled with 1 ml of solution to be tested, as shown in Figure 4.2.1. The solutions to be tested were: 1) citrate solution made with 2 ml of citrate mixed with 100 ml of distilled water; 2) 10 nm silver particles in borohydride solution with a

concentration of 1.97×10^{13} particle/ml; 3) 50 nm silver particles in citrate solution with a concentration of 1.57×10^{11} particle/ml. 4) borohydride solution made with 300 ml of borohydride mixed with 100 ml of distilled water; The plants were positioned in cuvettes so that the stems would not interfere with the spectrophotometer beam. Reference cuvettes with the same test solutions but without plants were also prepared and used in this experiment.

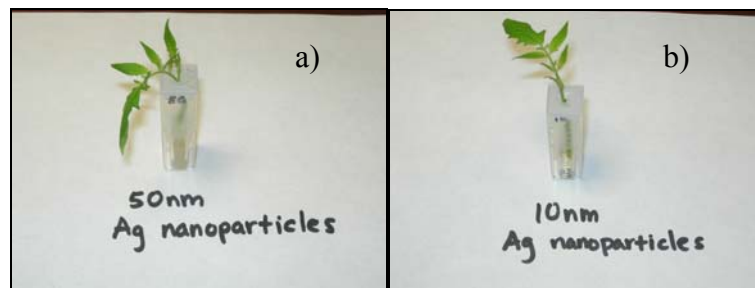


Figure 4.2.1. a) Tomato plant in a cuvette filled with 1mL of citrate solution of 50 nm silver nanoparticles; b) Tomato plant in a cuvette with 1mL of borohydride solution of 10 nm silver nanoparticles.

The tomato plants and the reference solutions were stored under natural lighting and at room temperature. This ensured transpiration-pull to provide the needed water and nutrient uptake within the 10 – 160 μ m diameter xylem vessels of the tomato stem (Van der Schoot, 2005). The UVS spectrum was obtained on each test solution several times over a 24-36 hour period. Before each UVS run, the cuvettes were gently vibrated to reduce clustering of silver nanoparticles and their attachment to the outside stem walls. The test cycle was repeated five times after which the plants appeared to stop absorbing silver nanoparticles. The test procedure for a cycle was as follows:

1. Take UVS scans right after the plant was placed in the cuvette or at the beginning of each subsequent cycle run.
2. Take UVS scans 6 hours after step 1;
3. Take UVS scans 24 hours or 36 hours after step 1;
4. If needed, refill the cuvettes to the beginning level with the test solutions and repeat steps 1-3 of the experiment as a new cycle.

The refilling procedures of the silver nanoparticle solution throughout this study were as the following as seen in Table 4.2.1.

Test Solution	Nanoparticle Size (nm)	Cycle #	Solution Added (ml)
2	10	1	1
2	10	2	0.4
2	10	3	0.2
2	10	4	1
2	10	5	1
3	50	1	1
3	50	2	1
3	50	3	0
3	50	4	1
3	50	5	1

Table 4.2.1. Refills performed in experiment

4.2.1 Citrate/Borohydride Control Test

An experiment was conducted on whether any chemical product of the tomato plant and citrate or borohydride reference solutions (test solutions #1 and #4) would react with the silver nanoparticles. A schematic of the test procedure is shown in Figure 4.2.1.1. A UVS spectrum was obtained on a citrate reference solution as shown in Figure 4.2.1.2a and on a borohydride reference solution as shown in Figure 4.2.1.2b. Cuttings from a tomato plant were placed in citrate and borohydride solutions for 24 hr. The plants were removed and 50 nm silver solution was added to citrate solution. In addition, 10 nm silver solution was added to borohydride solution and UVS spectra immediately taken. Thirty six hours after the nanoparticles introduction another UVS scan was performed. All spectra are shown in Figure 4.2.1.3.

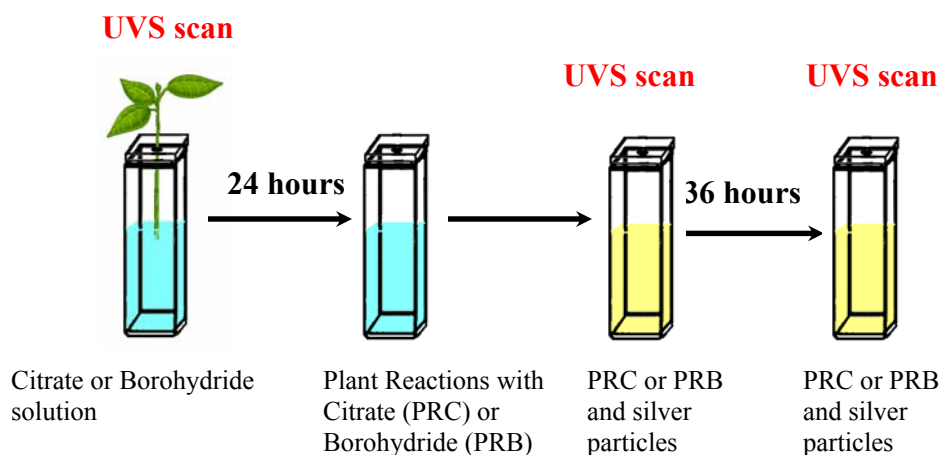


Figure. 4.2.1.1. Schematic of citrate/borohydride control test.

There was no evidence of a detrimental reaction product between the plant and the citrate solution or borohydride that would affect the silver nanoparticles. The absorbance wavelengths and peaks of the UVS spectra are identical for spectrums taken 36 hours apart as shown in Figure 4.2.1.3a and b.

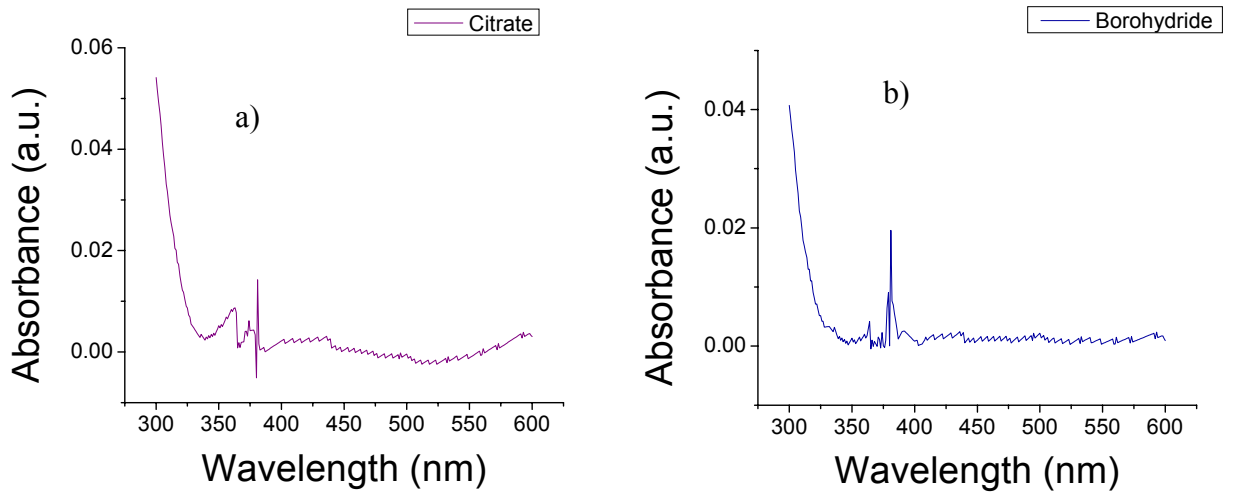


Figure 4.2.1.2. a) UVS spectra of pure citrate solution. b) UVS spectra of pure borohydride solution.

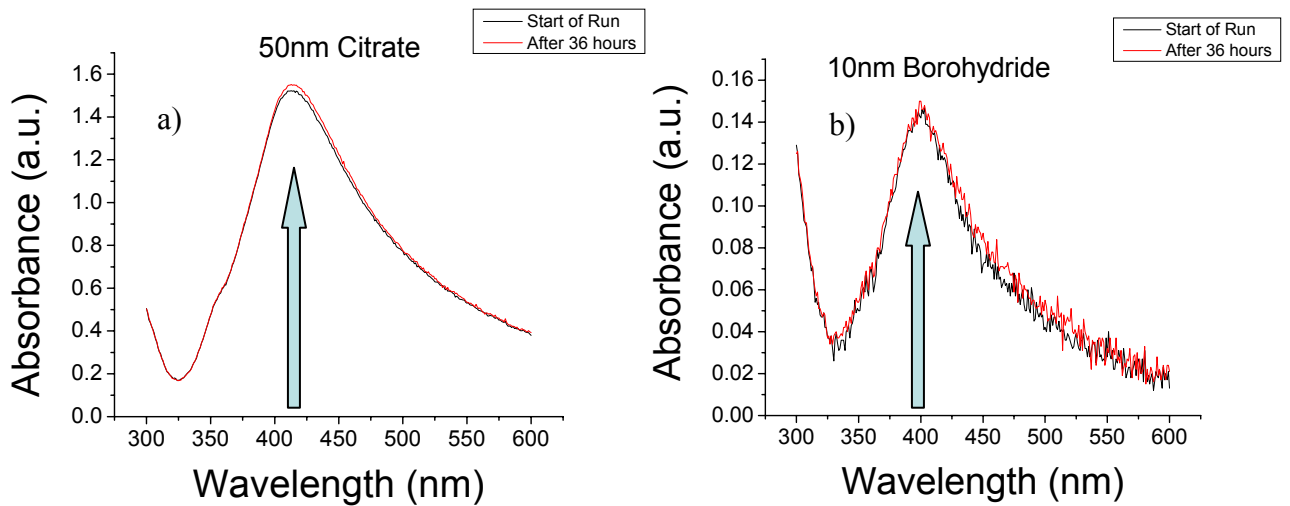


Figure 4.2.1.3. a) UVS spectra of 50 nm silver particles in plant immersed citrate solution using the sequence shown in Figure 4.2.1.1. b) UVS spectra of 10 nm silver particles in plant immersed borohydride solution using the sequence shown in Figure 4.2.1.1.

5. RESULTS AND DISCUSSIONS

5.1 Experimental Results

UVS and Raman Spectroscopy were used to monitor the uptake of silver nanoparticles by the tomato plants and the distribution of the particles within the plants. The effect of the silver nanoparticles on the tomato plant was visually observed. The UVS spectra from each test cycle are shown in Figure 5.1.1 through Figure 5.1.5. The UVS spectra were taken from samples and references at different times, as described in section 4.2. The data in Figure 5.1.1 shows that in the first 6 hours the concentration of silver nanoparticles in the cuvettes decreased by a significant amount as indicated by the height of the absorption peak while there was no change in the reference solutions. This indicates that the silver nanoparticles are either being taken up by the tomato plant or are collecting on the plants' stems. It is assumed as uptake by the plant because of moderate vibration performed to prevent collection on the stem. It is also evident that the location of the absorption peak shifted towards the long wavelength. Visual observation during this run showed that the color of both the 10 nm and 50 nm silver particle solutions changed to slightly clear in color, but no physical change in the plants was observable.

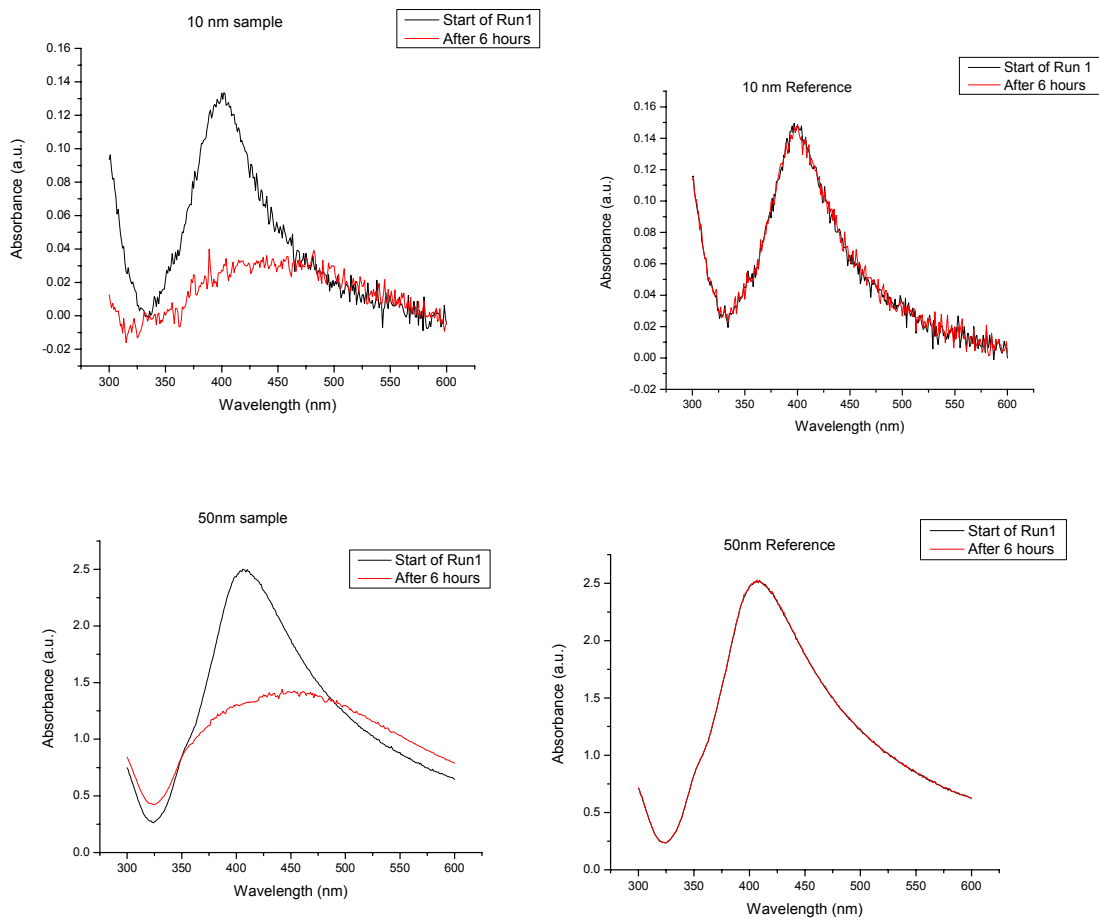


Figure 5.1.1. Cycle 1, UVS spectra of tomato plant samples in 10 nm and 50 nm Ag nanoparticles solutions and reference solutions.

In cycle 2, corresponding data as seen in Figure 5.1.2 shows a reduction in the absorbance peaks as was observed in cycle 1, but magnitude of the reduction in cycle 2 is much smaller compared to cycle 1.

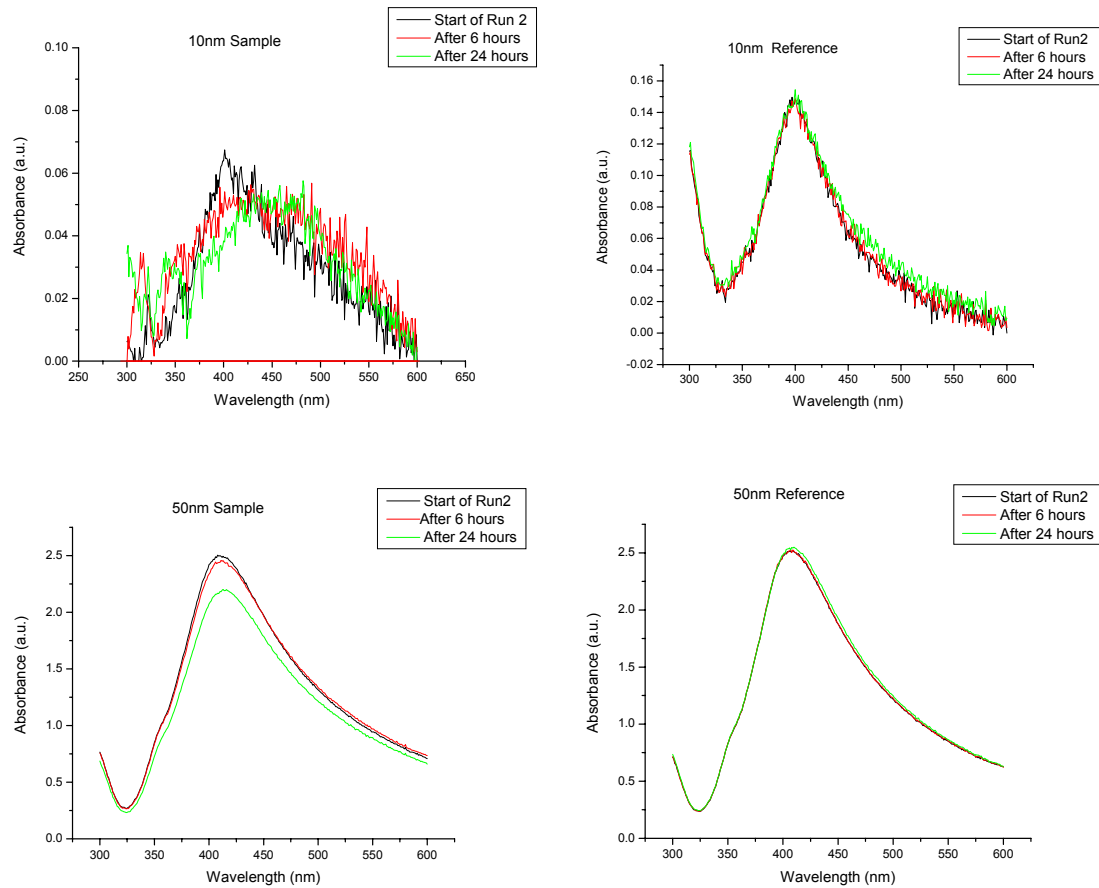


Figure 5.1.2. Cycle 2, UVS spectra of tomato plant samples in 10 nm and 50 nm Ag nanoparticles solutions and reference solutions.

In cycle 3, corresponding data as shown in Figure 5.1.3, the 10 nm silver particle solution showed a greater reduction in the absorption peak than the 50 nm silver particle solution. Visually, the plant in the 10 nm silver particle solution began to turn brown at the tip of the stem, but the plant in the 50 nm silver particle solution did not show any observable color change and even began growing small leaves.

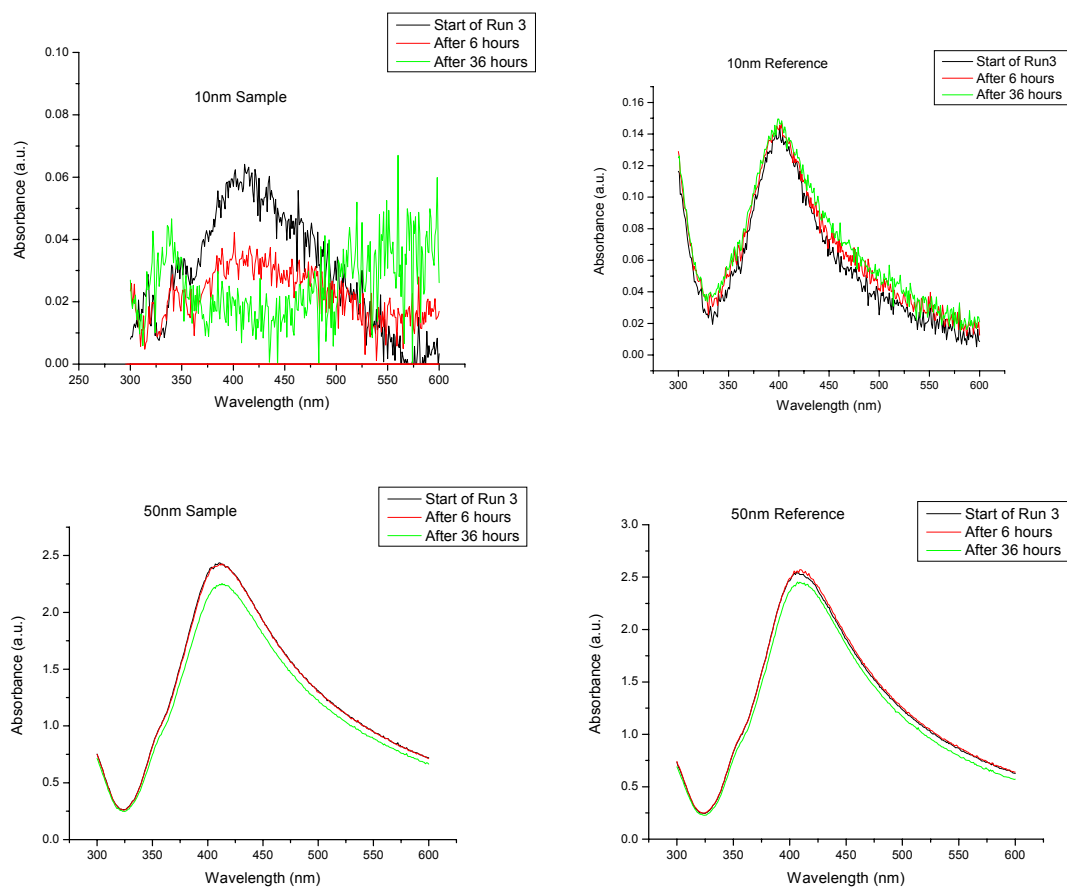


Figure 5.1.3. Cycle 3, UVS spectra of tomato plant samples in 10 nm and 50 nm Ag nanoparticles solutions and reference solutions.

In cycle 4, shown in Figure 5.1.4, the absorbance peak decreased for the 10 nm silver particle solution but increased in the 50 nm silver particle solution. Also, the reference solutions of both silver nanoparticle solutions in this run showed an increase in the absorbance peaks, which would be likely due to small clustering of the nanoparticles over time. The stem continued turning brown farther up the plant in the 10 nm silver particle solution.

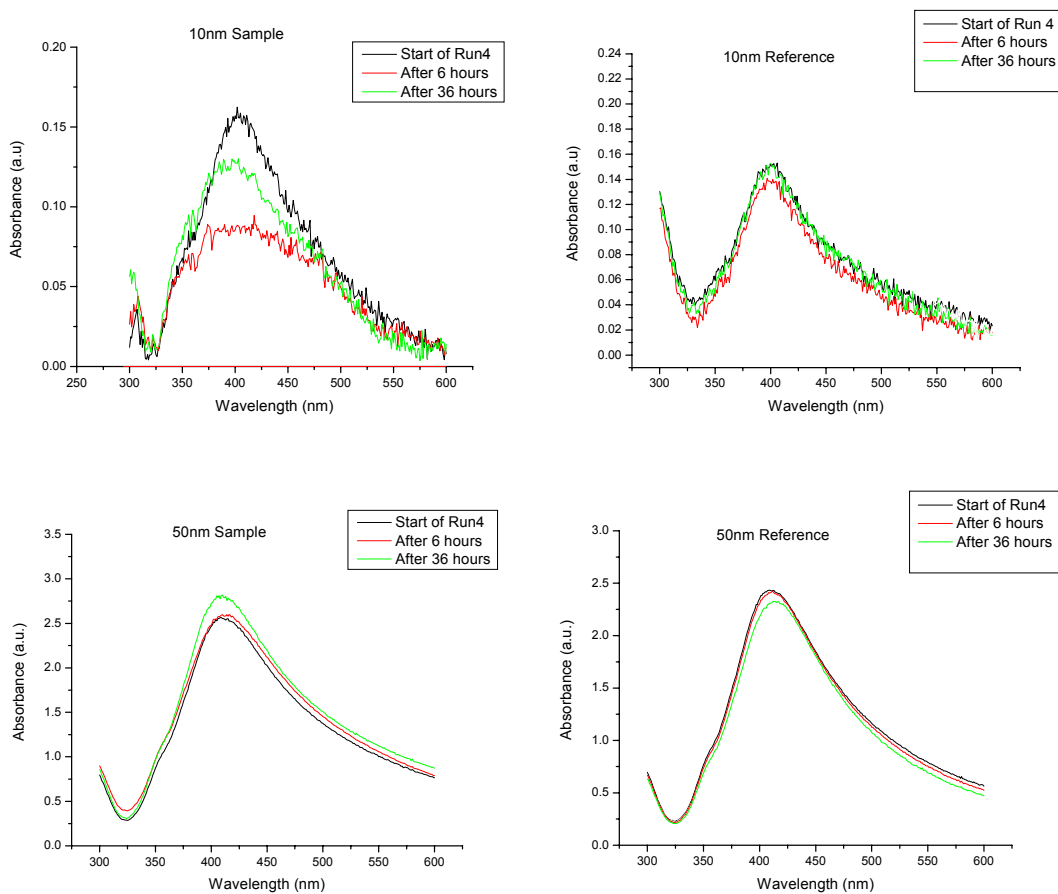


Figure 5.1.4. Cycle 4, UVS spectra of tomato plant samples in 10 nm and 50 nm Ag nanoparticles solutions and reference solutions.

In cycle 5, shown in Figure 5.1.5, the absorbance peaks of the 10 nm silver solutions had a very small decrease, and the 50 nm silver particle solutions began to resemble the reference. This shows that the plants may not take up nanoparticles due to the death of the plant or the plants may have reached their saturation point. The leaves of the plant in 10 nm silver solution, began to wither and turned brown.

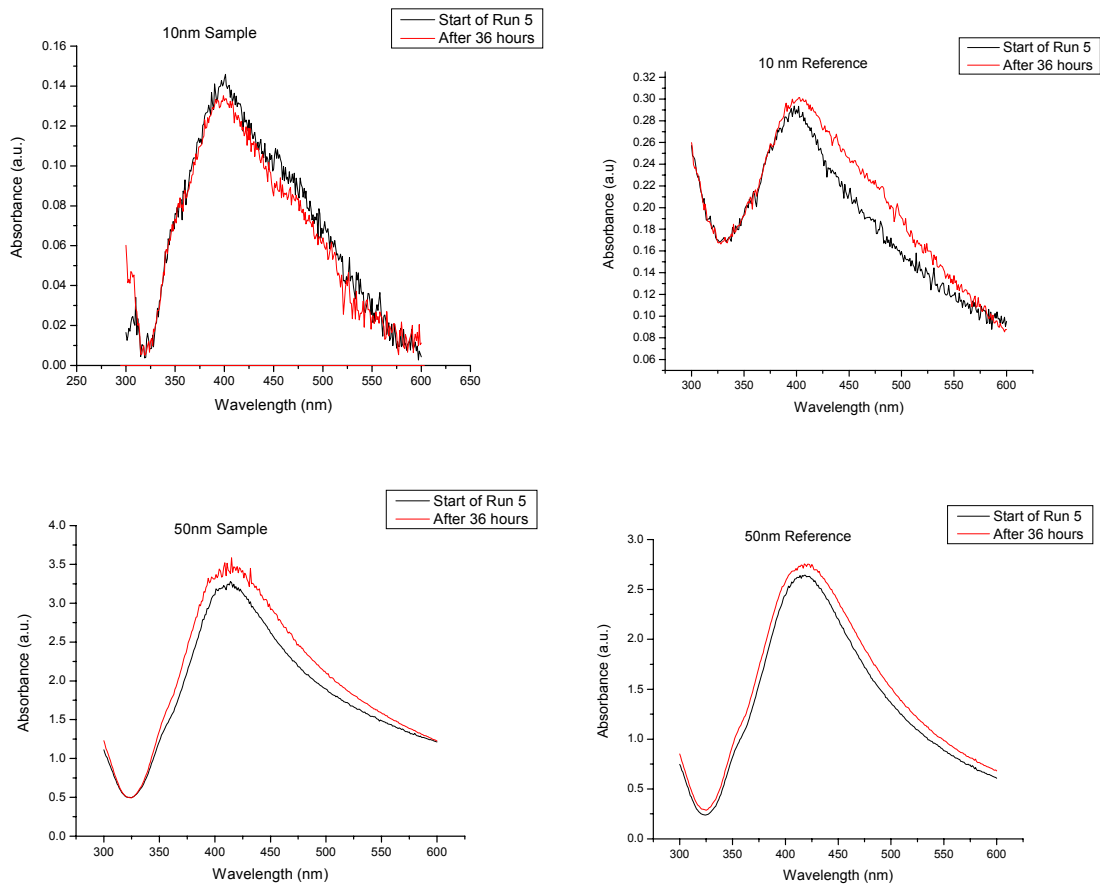


Figure 5.1.5. Cycle 5, UVS spectra of tomato plant samples in 10 nm and 50 nm Ag nanoparticles solutions and reference solutions.

The plant in 50 nm silver particle solution looked healthy throughout the test and continued to grow. The plant in the 10 nm silver particle solution began dying and eventually died after cycle 5. Figure 5.1.6 displays an image of the samples and references after cycle 5. From left to right, the samples are the 10 nm reference, 10 nm sample, 50 nm sample, and 50 nm reference.

This experiment was repeated three times with six different samples and results were very similar to what is reported above, confirming the results.

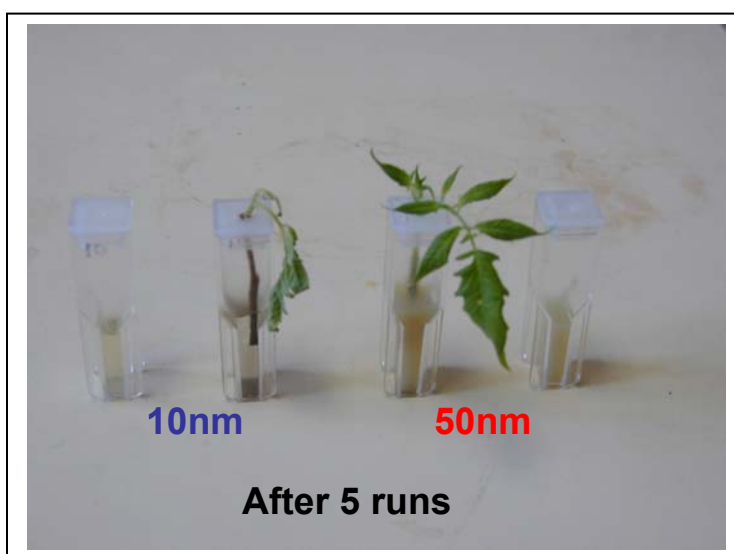


Figure 5.1.6 Image of samples and reference

After cycle 5 of the UVS test, the leaves of the plants were analyzed for silver nanoparticles using Raman Spectroscopy, but a good output spectrum above 0.1% of the power of the light source at a wavelength of 514 nm was not achievable because of high intensity scattering on the detector. Previous Raman spectra were achieved at 5 % of the power of the light source at a wavelength of 514 nm. The high intensity scattering is likely due to the leaves being saturated with silver nanoparticles. The Raman spectra are shown in Figure 5.1.7 below.

Raman Spectra of tomato plants leaves after UV/vis run 5

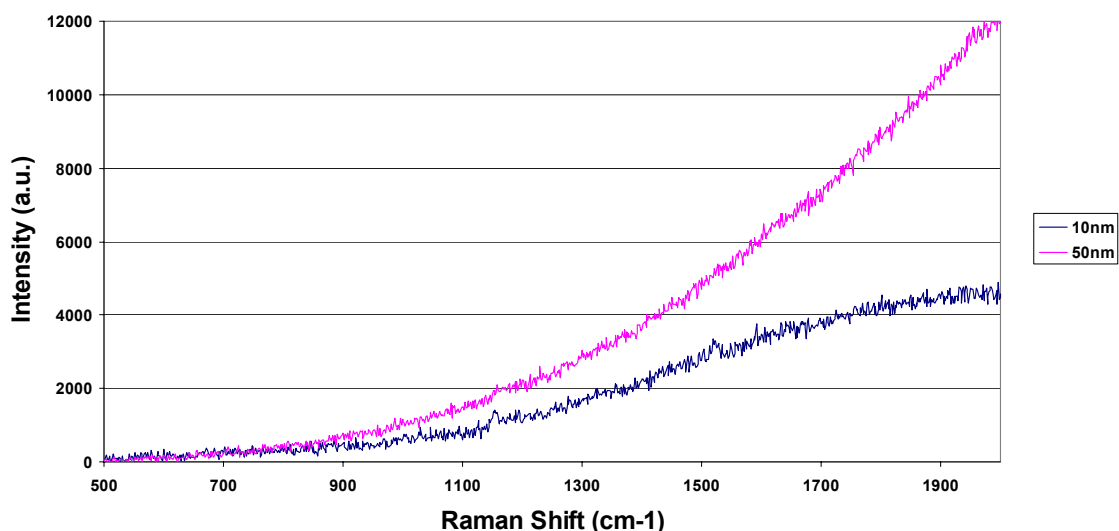


Figure 5.1.7 Raman spectra of leaves after UVS cycle 5 with 0.1% of power of 514 nm light source.

5.2. Conclusions

This study showed several approaches in determining whether tomato plants uptake silver nanoparticles and if the silver nanoparticles have an affect on the plant growth. When tomato plants were exposed to silver nanoparticles, the concentration of nanoparticles within the solution decreased with time, which indicated the uptake of nanoparticles by the tomato plant. It is also found that the 10 nm particles have a stronger or faster influence on the plants than the 50 nm particles. Raman spectroscopy showed that silver nanoparticles were present in the stems of the plants, meaning that they were absorbed through the roots at a slow rate. However, by removing the roots for the UVS experiments, the uptake rate of silver nanoparticles was increased.

Based on the concentration change obtained from the UVS spectra displayed in Figures 5.2.1 and 5.2.2 below, combined with the visual observation of the plant growth, we may conclude: 1) the smaller the silver nanoparticles, the faster the uptake by the tomato plant through its stem, and 2) the absorption (uptake) of silver nanoparticles by the tomato plant results in the death of the plant. It must be recognized that the death of the plant as presented in the UVS test may not be the same results if the tomato plants had roots.

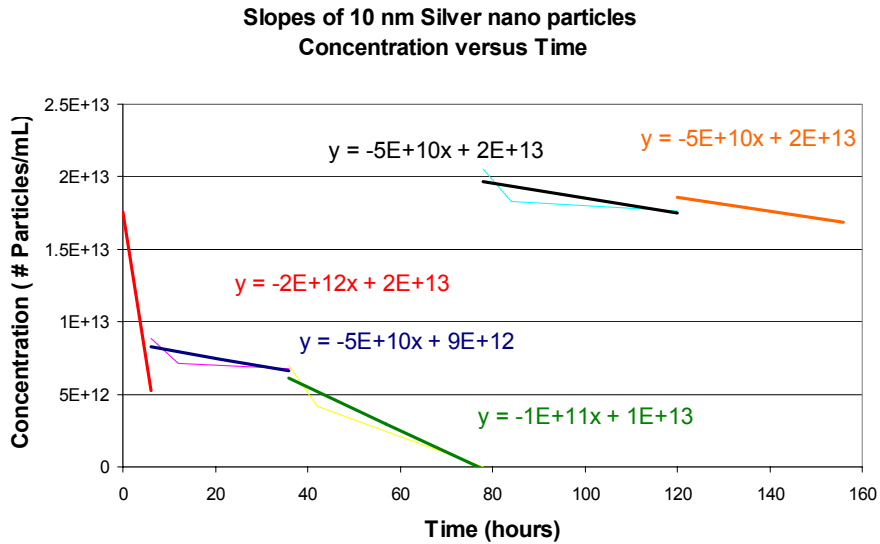


Figure 5.2.1. Slopes of 10nm Ag nanoparticles uptake in tomato.

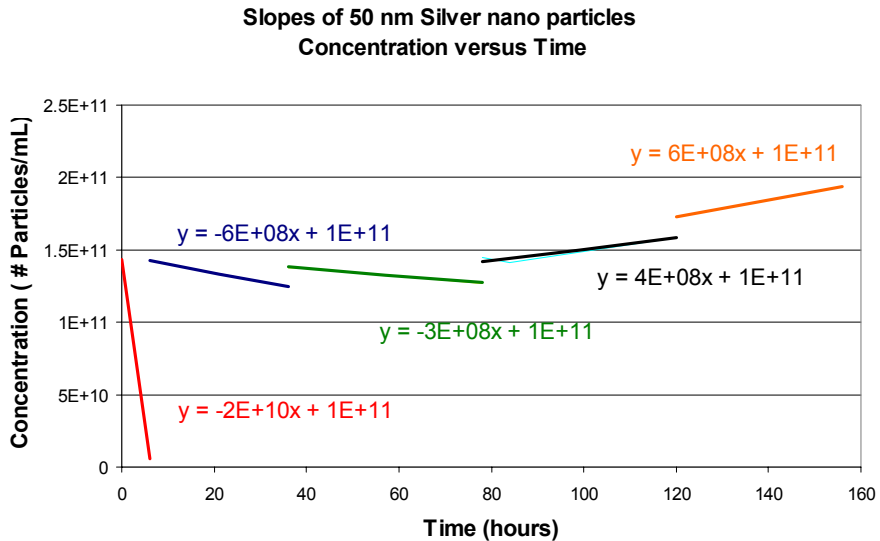


Figure 5.2.2. Slopes of 50nm Ag nanoparticles uptake in tomato.

6. FUTURE WORK

Future work must be done to discover the mechanism that is happening inside the plant that causes the deadly effect. The determination of how small the size of the silver nanoparticle has to be to cause it to be toxic to the tomato plant also must be attempted.

7. PLANT MONITORING SYSTEM

Smart Agriculture is based on real-time monitoring of crops and fields to optimize plant growth. To effectively achieve smart cultivation it is essential that the needs and issues of the plant are met in a timely manner. Common issues most plants encounter are insect infections, droughts, improper pH in soil and/or solution, diseases/mold, exposure to harsh weather conditions, and late harvesting. Sensor networks and data acquisition systems play a significant role in establishing these needs and issues so that a swift reaction to make the proper provisions can occur. However, there are many disadvantages with current sensor networks and data acquisition systems, such as their short battery life, narrow temperature ranges, and numerous wire connections. Current sensor networks also tend to output minute signal responses, making them difficult to detect. Wireless communication can be used as a solution for the numerous wired connections between data acquisition systems and monitoring stations, as well as to increase the communication distance between the two. Figure 7.1 is a diagram illustrating the concept of Smart Agriculture with wireless communication.

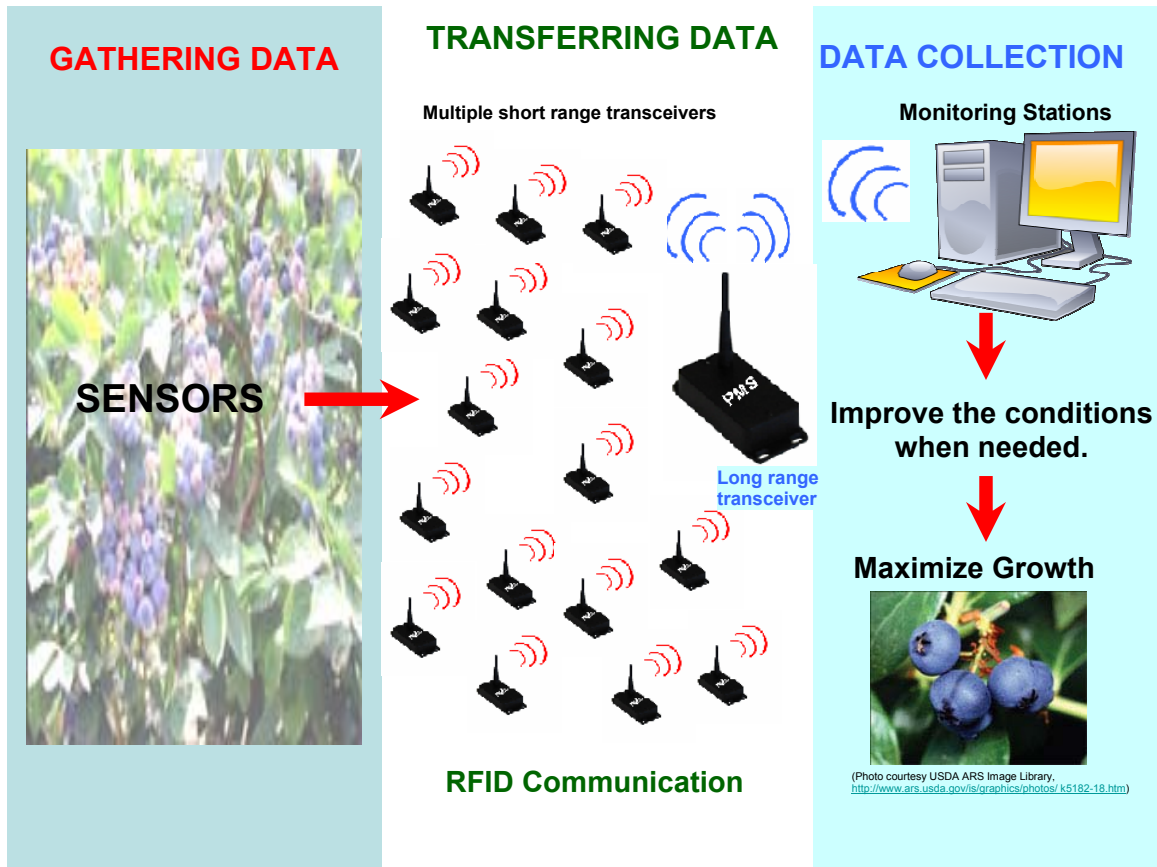


Figure 7.1. Illustration of the concept of Smart Agriculture with wireless communication

8. OBJECTIVES OF RESEARCH

The objective for the Plant Monitoring System (PMS) research is to develop a monitoring system that will track soil temperature, soil moisture, insect infestation, and fruit ripening via a wireless system. This system will in turn help maximize plant growing conditions, product yield, and product quality. The system will take readings from a network of sensors, recording everyday conditions of the plant's environment, keeping close watch on issues that might be harmful to the plant's growth. The system will output the recorded data in a useful format so that the user can make swift provisions. Ultimately, the system will be a low-cost, portable, long life battery-powered (~10 years), user-friendly, multi-sensor, plant monitoring system that operates between the temperatures of -50 °C and 80°C.

9. CIRCUIT DESIGN

A circuit was designed to produce a low-cost, portable, battery-powered, user-friendly, and multi-sensor plant monitoring system to perform the data acquisition. The process for circuit design began with a block diagram of the system and then component selection to meet the various criteria. Below is a block diagram of the PMS (Figure 9.1). Showing the major modules of the system.

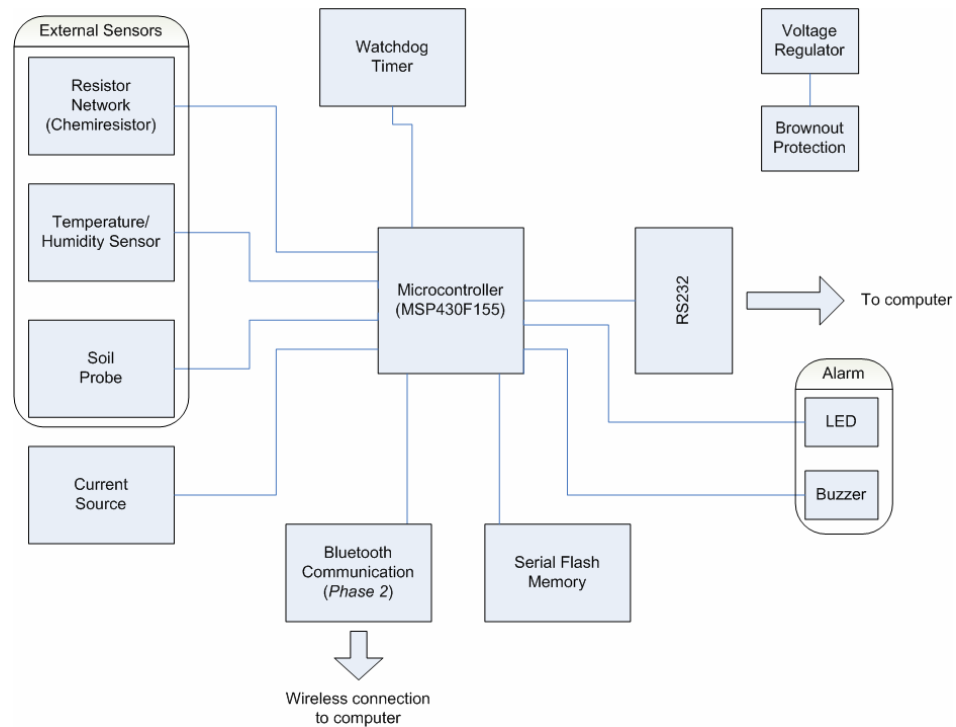


Figure 9.1 – Block diagram of PMS

The microcontroller was the key component of the system that was carefully selected from the thousands of industry devices. The microcontroller was required to meet all specifications set for the system. The wireless communication module also needed the same care in its selection. The other modules of the system were readily available and generally met the necessary specifications.

9.1 Microcontroller Selection

Microcontrollers are self-contained computers on a chip. They contain a CPU (central processing unit), fixed and variable memory, serial and/or parallel interfaces, data acquisition circuits, special timers, and various other circuit blocks. There are thousands of microcontrollers provided by many manufacturers. Each manufacturer has its own architecture variation and programming instruction sets. With so many varieties of architectures available and unique instruction sets, each microcontroller could rightly belong to a category of its own. This is why selection of a microcontroller must be done with care so that it operates as needed.

Temperature range and low-power consumption were major issues that were considered for the PMS. Typically, most manufacturers guarantee operation in the temperature range of -40 to 85 °C. The PMS goal of operation between -50 to 80°C limited the available microcontrollers. An intensive search for microcontrollers was conducted. This search led to two leading microcontroller manufacturers: Texas Instruments (TI) and Atmel. Table 9.1.1 displays a list of the microcontrollers' operational specifications. The manufacturers only provided specifications for operation at 25°C and 85 °C.

The TI MSP430F155 microcontroller was chosen based on the provided data, for its lower power consumption in sleep and power save modes compared to the other microcontrollers. The selected microcontroller was tested for operation at -50°C to 80 °C; the results are given later in the result section.

Power Save Current Consumption with 32 kHz Running

Manufacturer	Device	Typical 2.2V @25°C	Maximum 2.2V @85°C
TI	MSP430F2131	1.1 μ A	6 μ A
TI	MSP430F155	0.8 μ A	2.3 μ A
Atmel	ATmega165P	0.65 μ A	NA

Power Down Current Consumption

Manufacturer	Device	Typical 3.0V/5.0V @25°C	Maximum 3.0V/5.0V @85°C
Atmel	78KO/Kx2 5.0V	NA / 1 μ A	NA / 20 μ A
Atmel	R8C/tiny 3.0/5.0V	0.7 μ A/ 0.8 μ A	3 μ A/ 3 μ A
TI	MSP430F2xxx	0.1 μ A / NA	3.5 μ A/ NA
TI	MSP430F1xxx	0.1 μ A / NA	1.9 μ A/ NA
Atmel	ATmega165P	0.1 μ A / 0.6 μ A	2 μ A/ NA

Table 9.1.1. List of selected low-power microcontrollers

9.2 Wireless Communication Selection

Wireless technologies have grown rapidly over recent years. This growth is partially due to the vast growth in the cell-phone industry (Wang et al., 2006).

The types of wireless protocols used range from simple IrDA that uses infrared light for short range point-to-point communications, to wireless personal area network (WPAN) point-to-multi-point communications such as Zigbee and Bluetooth, to long-distance cellular phone systems, such as Global System for Mobile communications (GSM) (Wang et al., 2006). A comparison of the different wireless protocols is shown in Figure

9.2.1. Although many industries are using wireless communication, the usage in agriculture and food applications are still rare.

Several wireless protocols were studied to select a wireless protocol that would closely meet the requirements of the PMS. Table 9.2.1 shows a list of wireless modules researched. Each protocol had its strength and weaknesses, WiFi's (802.11 a, b,g,) power consumption and other important features did not meet the needed specifications. For example, its typical range is up to eight kilometers for transmitting and receiving, exceeding the needed range and requiring too much power for transmitting that distance. Bluetooth (802.15.1) has a moderately high current draw to transmit and receive, though it would have been acceptable. Also, the distance for a class 1 Bluetooth system seems reasonable, with a range of 100 meters (over 300 ft.). However, since it is limited to only seven nodes for devices to be connected it does not meet the criteria for multi-sensors in a large crop field. Alternatively, Zigbee (802.15.4) offers low power consumption, has an operating range of more than 100 meters (approx. 300 ft.) with line of sight communication, and has the ability to connect to 255 devices at once with minimal cross talk.

The list of devices was narrowed down to one or two devices from the Zigbee, Bluetooth and WiFi groups for further comparison. From the Zigbee group, Atmel's AT86RF210 was selected because of its low power consumption and large node connectivity of the device. From the Bluetooth group, Texas Instruments' BRF6150 was selected because it had the lowest power consumption of the group, even though its range presented a challenge. Within the Bluetooth group, National Semiconductor's LMX5252 was also selected. It had a slightly higher current consumption than the BRF6150, but its

range was far greater. From the WiFi group, Cirronet's WIT2410 was selected. It has the lowest current consumption in the WiFi group, but its current was still much higher compared to the currents used by the devices selected from the other two groups.

Based on the study and comparison of the RF modules gathered for this analysis, the initial protocol chosen was Zigbee Atmel's AT86RF210. Later, a shift was made to Bluetooth Texas Instruments' BRF6150 because of its popularity and adaptability and Zigbee's lack of technical support. The Bluetooth module is displayed in Figure 9.2.2.

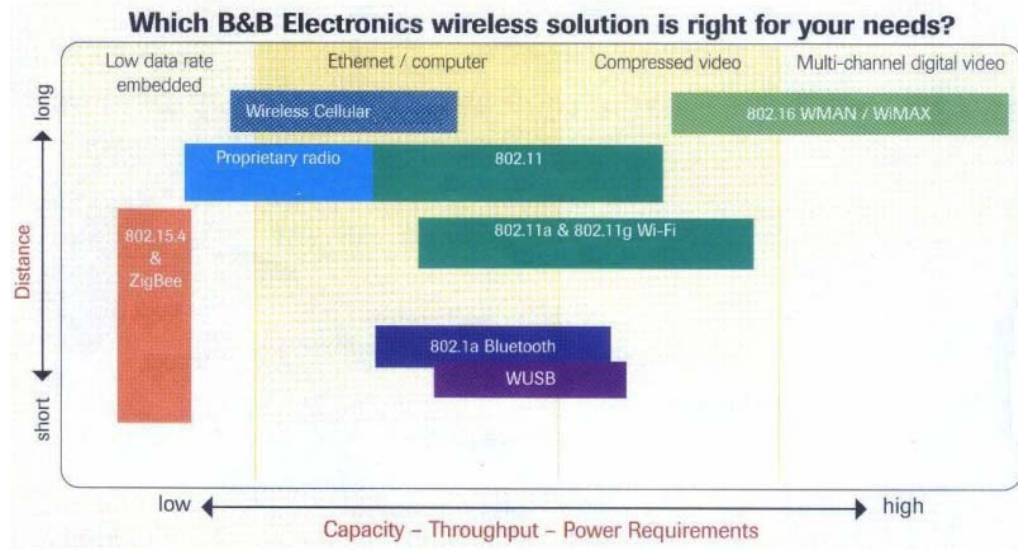


Figure 9.2.1. Comparison of the different wireless protocols (www.BB-elec.com)

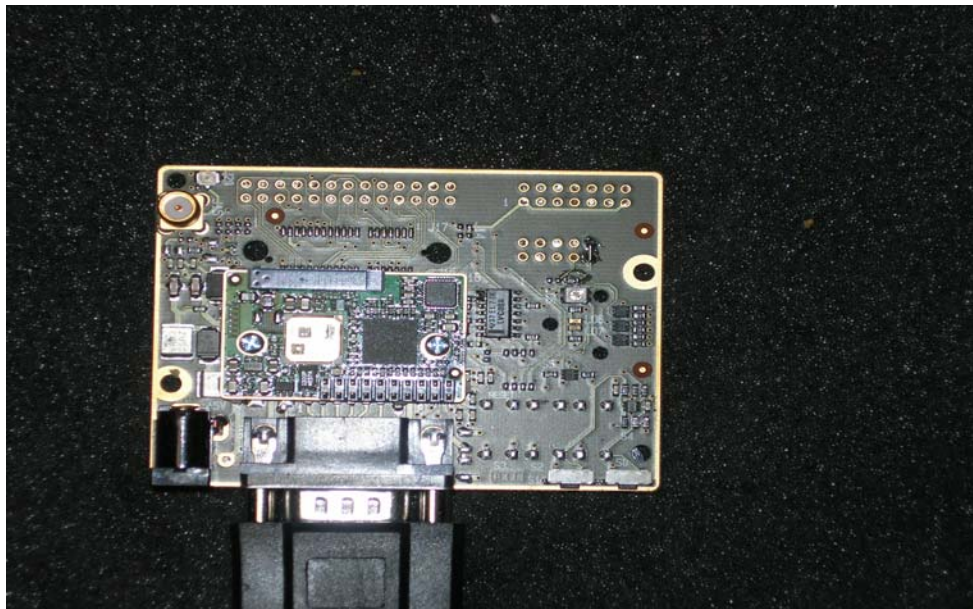


Figure 9.2.2. Bluetooth Module

ZigBee

ITEM	TECHNOLOGY	MANUFAC	PART#	DESCRIPTION	POWER SUPPLY (V)	RX CURRENT DRAW (mA)	TX CURRENT DRAW (mA)	SLEEP CURRENT (A)
1	ZIGBEE MODULE	ATMEL	AT86RF210	TRANSCEIVER	1.8-3.6	14.5	14.5	1x10 ⁻⁶
2	ZIGBEE MODULE	EAZIX	EZZB01	TRANSCEIVER	3.3	32	32	30x10 ⁻⁶
3	ZIGBEE MODULE	CIRRONET	ZMN2400	TRANSCEIVER	2.7-5.5	30	35	25x10 ⁻⁶
4	ZIGBEE MODULE	CIRRONET	ZMN2400-HP	TRANSCEIVER	3.3-5.5	50	150	25x10 ⁻⁶
5	ZIGBEE MODULE	IWT	AXON	TRANSCEIVER	3.3-6.0	21	19	140x10 ⁻⁶
6	ZIGBEE MODULE	CHIPCON	CC2420	TRANSCEIVER	2.1-3.6	19.7	17.4	20x10 ⁻⁶
7	ZIGBEE MODULE	FREESCALE	MC13191	TRANSCEIVER	2.0-3.4	45	38	150x10 ⁻⁶
8	ZIGBEE MODULE	PANASONIC	PAN802154HAR00	TRANSCEIVER	2.2-3.4	40	35	100x10 ⁻⁶
9	ZIGBEE MODULE	Telegesis	ETRX1	TRANSCEIVER	2.7-3.6	30	30	15x10 ⁻⁶
10	ZIGBEE MODULE	MAXSTREAM	XBEE	TRANSCEIVER	2.8-3.7	50	45	10x10 ⁻⁶
11	ZIGBEE MODULE	MAXSTREAM	XBEE-PRO	TRANSCEIVER	2.8-3.7	55	270	10x10 ⁻⁶

Bluetooth

Item	Technology	Manufacturer	Part #	Description	Power Supply	RX Current Draw	TX Current Draw	Sleep Current Draw
1	Class 1	Parallax	30068(eb500)	Transceiver	5-12VDC	25-35 mA	25-35 mA	3mA
2	Class 2	Texas Instr.	BRF6150	Transceiver	2.7-5.5 V	37 mA	25 mA	30uA
3	Class 1	National Semi	LMX5252	module	2.5-3.0 V	<60 mA	<60 mA	-
4	Class 1	Socket Comm	KwikBlue BC02	module	3.0-3.5 V	-	160 mA	<100 uA
5	Class 1	Initium	ESD01	Module	3.3 V	26 mA	72.7 mA	3 mA
6	Class 1	Roving Networks	Blue Port II	Module	3.3 VDC	-	40 mA	1 mA
7	Class 1	ALPS Electric	UGXZ5	Module	3.3 V	-	-	-

802.11 (WIFI)

Item	Technology	Manufacturer	Part #	Description	Power Supply	RX Current Draw	TX Current Draw	Sleep Current Draw
1	WiFi	Broadcom	BCM4317	Tranceiver	-	-	-	-
2	WiFi	Cirronet	WLN8-AN-DP101	Module	3.3 VDC	350 mA	420 mA	75 mA
3	WiFi	Cirronet	WIT2450	Tranceiver	3.3-10 V	40 mA	150 mA	-
4	WiFi	Cirronet	WIT2410	Tranceiver	3.3-10 V	22 mA	90 mA	< 50 uA
5	WiFi	Maxim	MAX2825	Tranceiver	2.7-3.6 V	119 mA	131 mA	38 uA
6	WiFi	Maxim	MAX2826	Tranceiver	2.7-3.6 V	148 mA	151mA	48 uA
7	WiFi	Maxim	MAX2827	Tranceiver	2.7-3.6 V	-	-	-

900MHz Wireless Modules

Item	Technology	Manufacturer	Part #	Description	Power Supply	RX Current Draw	TX Current Draw	Sleep Current Draw
1	912.00MHz	Rf Digital	RFD21130	Module	-	-	-	-
2	FHSS	Cirronet	WIT910	Module- RS232 Interface	3.3 VDC	100 mA	100 mA	250 uA
3	FHSS	Aerocomm	AC4790	Tranceiver- 3V TTL Serial Interface	3.3- 5 V	68 mA	68 mA	-
4	FHSS	Xstream	900Xstream	Tranceiver	5 V	50 mA	140 mA	< 26 uA
5	900MHz	Radiotronics	WI.232DTS	UART interface Tranceiver	5 V	-	-	-
6	FHSS	Radicom	WHM900	Tranceiver- 3V TTL Serial Interface	3.0-3.6 V	28 mA	36mA	4 mA

Table 9.2.1. List of wireless technology modules and their parameters

9.3 Board Layout

After components were chosen, a schematic diagram of the circuit board was made to show how the components were connected electrically to operate as a system. This required that each component's characteristics be studied to make sure that they met the temperature and stability requirements and that they were connected according to their interface requirements. Connectors had to be chosen and mounted so that power, the development system, and other input/output devices could be connected. It was also necessary to keep in mind how the system's power and other parameters would be measured once the unit was assembled.

The circuit board was designed and the layout was completed in Orcad board layout software. In order to design the board, each component's mechanical size was determined and a mounting "footprint" with the proper spacing and hole sizes was selected from an existing list; otherwise a new footprint was designed. Next, components were placed on the board so that copper etch connections could be made between component pins. Finally this design was converted to machine readable format so that a prototype printed wiring board (PWB or PCB) could be made. The PWB is bare boards made of an insulator of fiberglass epoxy with a copper etch pattern and holes. After this board was received, parts were soldered onto the PWB so that the prototype board (assembly) could be tested. The prototype board is shown in Figure 9.3.1 below. One of the main parameters that must be met was power consumption. Power consumption was measured by inserting a digital multimeter (setup for current measurements) into the wire between the external power supply and the board. The power consumption of the device

is shown in Table 9.3.1, the circuit board schematic is shown in Figure 9.3.2, and the Bill of Material is shown in Table 9.3.2 below.

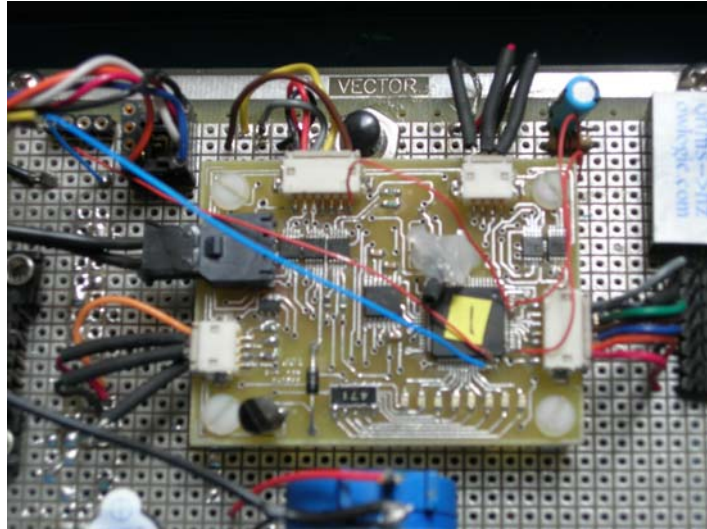


Figure 9.3.1. PMS prototype board

PMS State	Current Draw
Sleep mode	~ 0.350 mA
Operational mode	~ 23.4 mA

Table 9.3.1. PMS power consumption

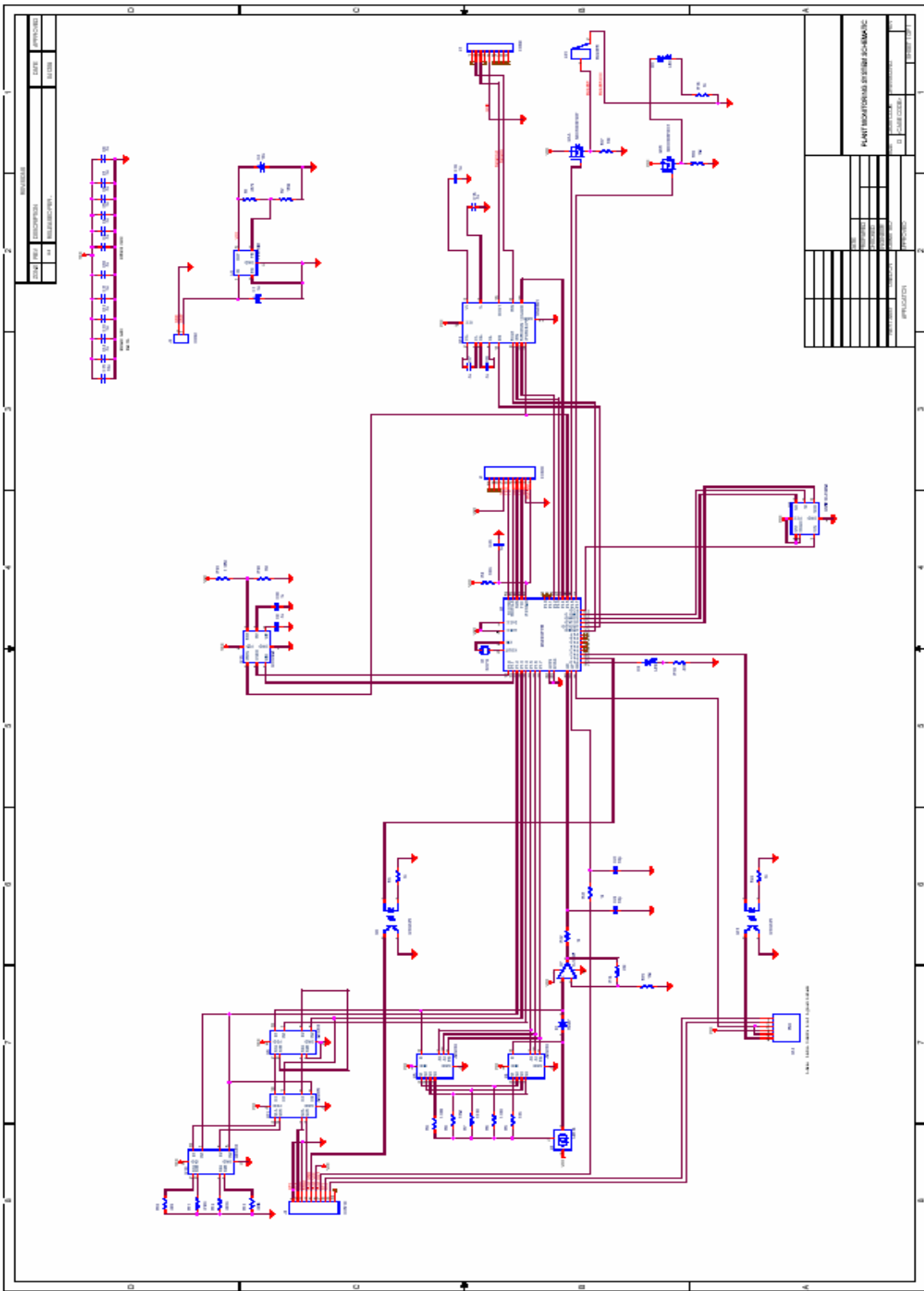


Figure 9.3.2. PMS circuit board schematic drawing

Item	Qty	Reference	Description	Manufacturer	Part Number
1	1	C1	Tantalum Capacitor, 0.1uF	Kemet	T491A104K035AS
2	1	C2	Tantalum Capacitor, 10uF	Kemet	T494B106K016AS
3	17	C3-C14,C16-C20	Capacitor, 0.1uF	Kemet	C0603C104M3RAC-TM
4	1	C15	Capacitor, 10uF	AVX	08056D106KAT2A
5	2	C22,C21	Capacitor, 10pF	AVX	06031A100KAT2A
6	1	C23	Capacitor, 1uF	Panasonic-ECG	ECJ-1VB1A105K
7	1	D1	Diode	Fairchild Semiconductor	1N457
8	1	D2	LED	Everlight	EL-19-21SURC/S530-A2
9	1	D3	LED	Everlight	743HD
10	1	J1	14 pin Connector	AMP	103309-2
11	1	J2	2 pin Connector	Molex	43650-0204
12	1	J3	DB 9 connector	AMP	747844-6
13	1	J4	10 pin Connector	3M	3M-10-RA
14	1	LS1	BUZZER	Projects Unlimited	AI155
15	1	Q1	Dual P-channel MOSFET	Fairchild Semiconductor	NDC7003P
16	1	R1	Resistor, 287kΩ	Vishay/Dale	CRCW0603287KFKTA
17	1	R2	Resistor, 169kΩ	Vishay/Dale	CRCW0603169KFKTA
18	5	R3,R18,R21,R22,R24	Resistor, 1kΩ	Vishay/Dale	CRCW06031K00FKTA
19	1	R4	Resistor, 100kΩ	Vishay/Dale	CRCW0603100KFKTA
20	1	R5	Resistor, 133Ω	Vishay/Dale	CRCW0603133RFKTA
21	1	R6	Resistor, 1.33kΩ	Vishay/Dale	CRCW06031K33FKTA
22	1	R7	Resistor, 13.3kΩ	Vishay/Dale	CRCW060313K3FKTA
23	1	R8	Resistor, 133kΩ	Vishay/Dale	CRCW0603133KFKTA
24	1	R9	Resistor, 1.33MΩ	Vishay/Dale	CRCW06031M33FKTA
25	1	R10	Resistor, 499Ω	Vishay/Dale	TNPW0603499RBETY
26	1	R11	Resistor, 4.99kΩ	Vishay/Dale	TNPW06034K99BEBD
27	1	R12	Resistor, 49.9kΩ	KOA Speer	RN731JLTD4992B25
28	1	R13	Resistor, 499kΩ	Vishay/Dale	CRCW0603499KFKTA
29	1	R14	Resistor, 20kΩ	Vishay/Dale	CRCW060320K0FKTA
30	3	R15,R16,R17	Resistor, 10kΩ	Vishay/Dale	CRCW060310K0FKTA
31	1	R19	Resistor, 470Ω	Vishay/Dale	CRCW0603470KFKTA
32	1	R20	Resistor, 1MΩ	Vishay/Dale	CRCW06031M00FKTB
33	1	R23	Resistor, 1.18MΩ	KOA Speer	RK73H2ALTD1184F
34	1	U1	Microcontroller	Texas Instrument	MSP430F1551PM
35	1	U2	Voltage regulator	Texas Instrument	TPS77001DBVR
36	1	U3	Adjustable Current Source	National Semiconductor	LM134H
37	2	U5,U4	4-to-1 analog multiplexer	Analog Devices	ADG704BRM
38	3	U6,U10,U11	Dual 2-to-1 analog multiplexer	Analog Devices	ADG836YRM
39	1	U7	Operational Amplifier	Texas Instrument	TLV2401IDR
40	1	U8	Serial flash memory	Atmel	AT25F1024AN-10SU-2.7
41	2	U15,U9	Optical switch	Omiron	G3VM-S5
42	1	U12	RS-232 Driver	Texas Instrument	MAX3221IPWR
43	1	U13	WDT/SVS	Texas Instrument	UCC2946D
44	1	U14	Soil Probe	Irrrometer	SMX
45	1	X1	32 kHz crystal clock	Vishay/Dale	XT38PA32.768KHZ

Table 9.3.2. PMS Bill of Materials

9.4 Software

This project required the use of the C programming language software. IAR Embedded Workbench IDE and Dev-C++ IDE were used for the C code programming environment. The MSP430 Serial Programming Adapter was used in programming the code from the software to the microcontroller chip. The MSP430 USB Debugging Interface and HyperTerminal were used for in-circuit debugging the code and chip to ensure proper operations. Collectively, all of the above software and devices were used in the development of the PMS' software functions.

The PMS development in C allows for fast program execution and small source code size. Essentially, the PMS has a primary source code file and several header files that serve as modules for the many functions of the system. The operating software is an interrupt-driven program that allowed for better power conservation and operation in low-power modes. The system software was designed in a modular fashion so that any problems that occurred could be easily assessed and updates could be easily made. Modular design is considered good programming practice since it allows changes to be inserted or deleted without affecting other parts of the program. The C-programming flow-diagram is shown in Figure 9.4.1 below.

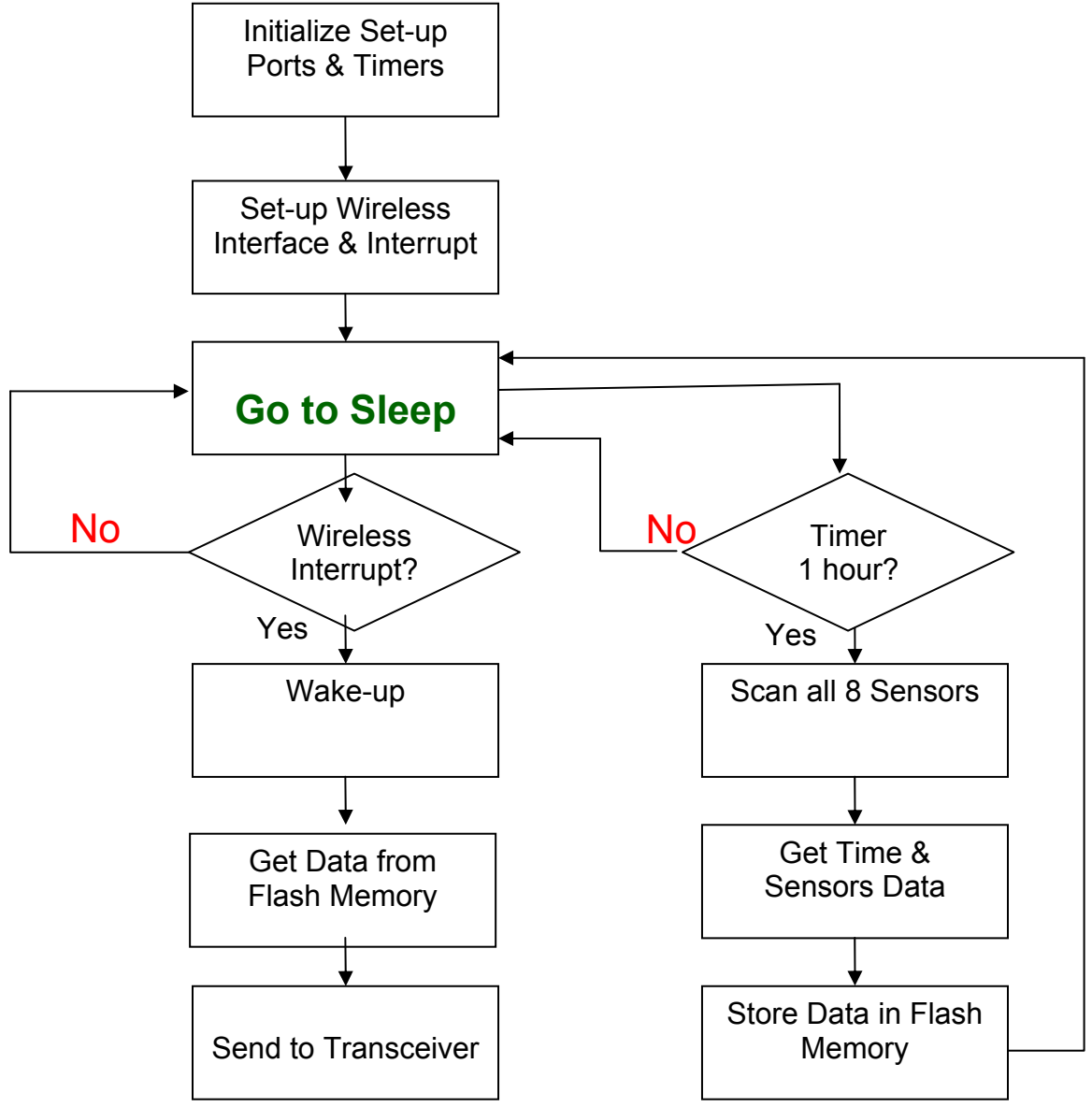


Figure 9.4.1. PMS C-programming flow-diagram

10. SENSING NETWORK

The PMS prototype sensing network is comprised of 4 sensors: a chemical-resistor, temperature and humidity sensors (bundled in one package), and a soil monitor. The chemical-resistor device changes resistance when exposed to a gas coming from nearby plants being eaten by insects or from plants in their ripening stages.

The temperature and humidity sensor were both part of a single package, a HIH-3602-C Relative Humidity (RH) sensor manufactured by Honeywell. Both relative humidity and temperature sensing were combined in a TO-5 housing with a hydrophobic sintered stainless steel filter. The laser trimmed thermoset polymer capacitive sensing elements had on-chip integrated signal conditioning. The temperature sensor was thermally connected with the RH sensor making the HIH-3602-C ideal for measuring dew point and other absolute moisture terms. Factory calibration data supplied with each sensor allowed individually matched downstream electronics and $\pm 2\%$ RH total accuracy. Sensor construction consisted of a planar capacitor with a second polymer layer to protect against dirt, dust, oils and other hazards.

The soil monitor was a granular matrix sensor made by Watermark, part number 200SS. It was an indirect, calibrated method of measuring soil water. Through an electrical resistance type sensor it could be read by data logging equipment or in our case, the plant monitoring system.

11. EXPERIMENTS

To investigate the basic operation of the PMS, two tests were performed. The first test was conducted to investigate two major functions of the system: 1) The system's ability to collect data as well as transmit the data to an external computer; 2) The proper operation of the sensor networks, namely to gather data that can be analyzed to ensure that plant growth of tomato plants could be sustained. Secondly, a temperature test was performed to obtain the maximum temperature operating range of the system. It should be noted here that the processor chosen for low power did not have specifications to cover the temperature range; thus, test was done to verify useable operation outside the specified parameters.

11.1 Set-up

A 20 gallon aquarium was filled with sand (Figure 11.1.1), and two tomato plants were transplanted into the aquarium, creating a simulated growing environment. Sand was used to see if the PMS was capable of assisting in tomato plant growth in one of the most difficult soils to grow plants in. The setup was monitored by a computer using HyperTerminal software via Bluetooth for several weeks. The Bluetooth transmitted shorter distances than expected. The output data was captured (Figure 11.1.2), during

fifteen minute intervals. Temperature, humidity, soil moisture and resistance of a variable resistor, simulating the chemical-resistor, were recorded. The output response of the temperature and humidity of the PMS was compared to the output of a commercial temperature/humidity device.

Several PMS devices were then placed into an environmental chamber, with each devices output signal monitored, to test the operation of the devices in the extreme temperature ranges (-50°C and 80°C). The chamber is shown in Figure 11.1.3.



Figure 11.1.1. Experiment Setup for PMS testing.

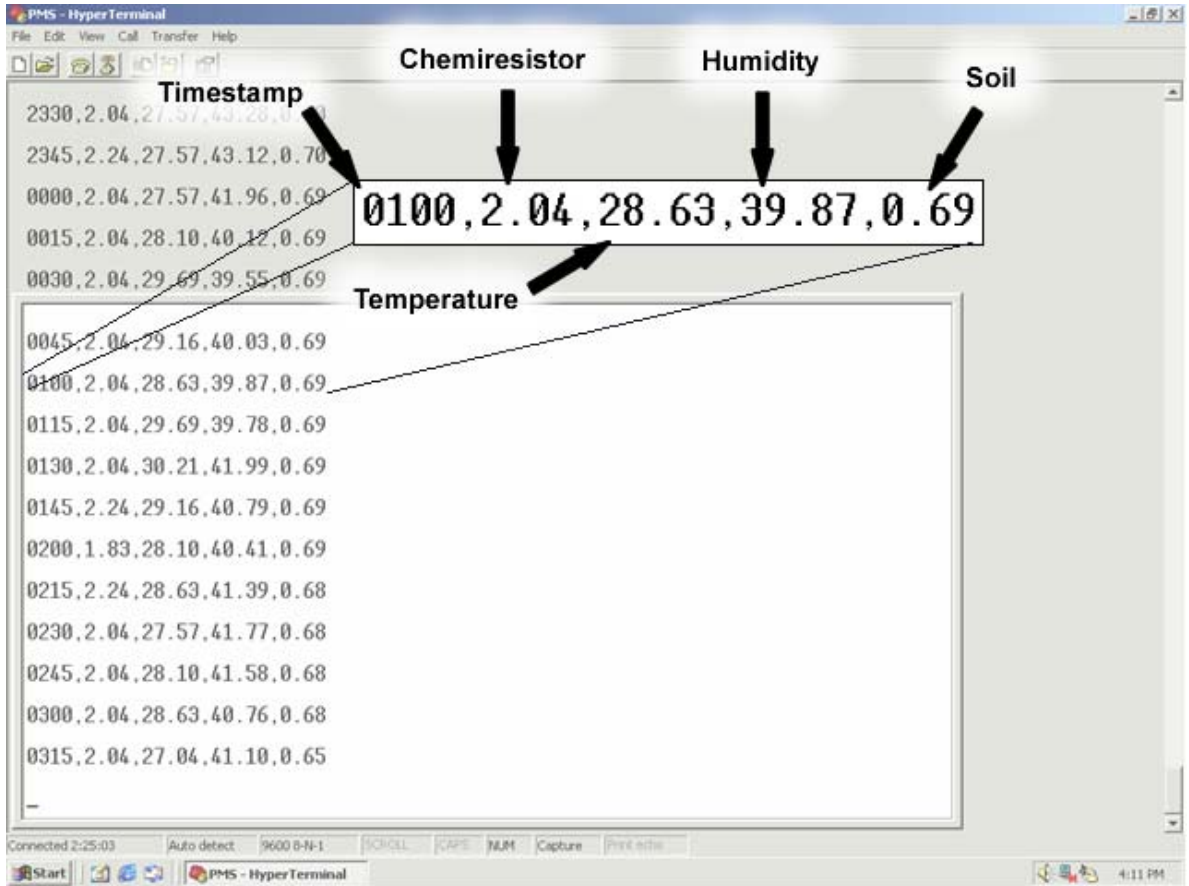


Figure 11.1.2. Screen print of HyperTerminal capturing PMS output data



Figure 11.1.3. Environmental chamber used for temperature test

12. RESULTS AND DISCUSSIONS

The PMS outputs data was taken in fifteen minute intervals. Hourly samples were taken from the recorded PMS data and compared with the recorded reference data. Data is shown in Table 12.1. From the experiment, the mean temperature reading for the PMS was ~ 25.74 degrees Celsius, while the mean reference temperature was ~ 25.66 degrees Celsius. The mean PMS humidity reading was ~ 45.05 %RH, while the mean reference humidity reading was measured at ~ 44.51 %RH.

The soil monitor was tested by saturating the soil with plant nutrients and then allowing the soil to dry as seen in Figure 12.1. To effectively show its proper operation, this process was drawn-out over 4 weeks. The soil monitor began to reach its driest state over a period of 5 days (under deliberate drying conditions). At this point, the soil was again saturated and allowed to repeat the cycle. During this period of time the tomato plants soil moisture needs were met and allowed for plant growth. Tomato plants wilt rapidly when the roots do not have enough moisture. Observation of the plants for wilting was used as the criteria to determine that moisture needs were met.

The results of the temperature test are displayed in Table 12.2. The TI microcontroller used in the PMS, stopped operating below the temperature of -45 °C but begin normal operation when the temperature was increased to -40°C. Although this board did not operate at the low temperature, it did recover once the temperature returned

to a higher temperature. Note that virtually no plants are cultivated at these cold temperatures. However, it could be used for monitoring storage temperatures of grains and other frozen foods. Several simple boards were fabricated using the Atmel Atmega165p and they passed both extremes.

Time	PMS Temp	PMS Hum	Ref. Temp	Ref. Hum
8:00 AM	25.98	47.48	24.46	45.82
8:15 AM	23.87	47.17	24.41	44.24
8:30 AM	24.4	46.76	24.82	44.24
8:45 AM	25.98	44.99	24.82	44.14
9:00 AM	26.51	47.42	25.81	47.9
9:45 AM	23.87	46.88	24.26	47.66
10:00 AM	24.4	48.87	24.8	49.62
11:00 AM	25.98	49.47	24.42	45.2
12:00 PM	27.57	44.48	27.9	44.03
1:00 PM	29.69	40.03	29.91	40.73
1:30 PM	26.51	40.09	27.41	40.79
2:00 PM	27.04	44.8	28.14	45.5
3:00 PM	27.04	43.19	24.96	42.27
3:45 PM	23.87	41.2	24.76	41.91
4:00 PM	23.34	42.9	24	43.6
Average	25.73666667	45.04866667	25.65866667	44.51

Table 12.1. Temperature and humidity data recorded (PMS and reference)

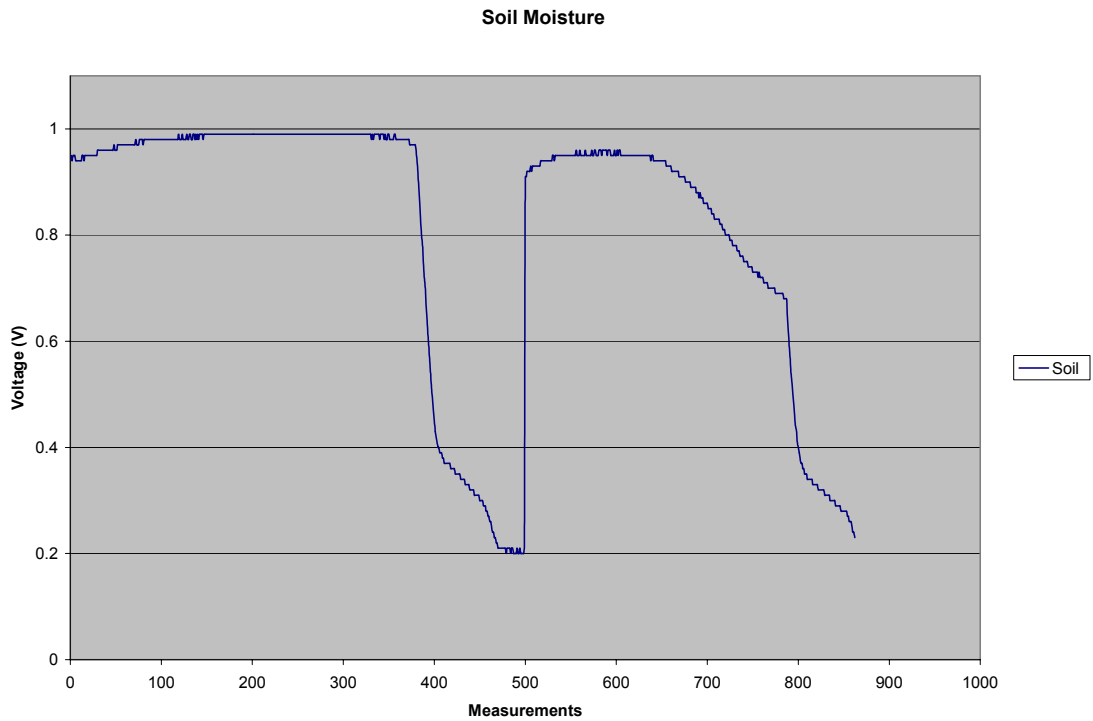


Figure 12.1. Graph of PMS soil readings [The soil monitor's voltage readings ranged from 0.2 Volts (dry) to 1.0 Volt (wet)]

Microcontroller	- 50°C	80°C
MSP430F155	Failed	Passed
ATmega165P	Passed	Passed

Table 12.2. Results of temperature extreme operation test

12.1 Conclusion

- The average temperature measurements were approximately 0.1 degrees from the reference while the average humidity measurements were seen to be about .54% off.
- Current draw of the PMS in sleep mode was low (~0.4 mA), but needs to be lower.
- The soil moisture sensor detected the plant moisture needs for 4 weeks helping in the growth of the plant.
- The TI MSP430F155 didn't operate in low end of temperature range needed.
- Bluetooth had short transmission distance.

In conclusion, the PMS unit responses performed reliably and can subsequently be used as a wireless smart agriculture device.

13. FUTURE WORK

Future work would be to develop a new system using the ATmega165P which operates in the temperature range needed. Also reduction of the current draw of system is a must, in the order of ($\sim 20 \mu\text{A}$). This would allow 10 year battery life of most standard batteries. The wireless communication protocol should be converted from Bluetooth to RFID, because RFID might provide longer communication capabilities. Finally, the system needs to be tested in the field for operation.

BIBLIOGRAPHY

- Elechiguerra J.L., Burt J., Morones J.R., Camacho-Bragado A., Gao X., Lara H.H., Yacaman M.J., (2005). Interaction of silver nanoparticles with HIV-I. *Journal of Nanobiotechnology* 3:6.
- Feng Q.L., Wu J., Chen, G.Q., Cui, F.Z., Kim, T.N., Kim, J.O., (2000). A mechanistic study of the antibacterial effect of silver ions on *Escherichia coli* and *Staphylococcus aureus*. *Journal of Biomedical Materials Research* 52, 662-668.
- Gardea-Torresdey J.L., Peralta-Videa J.R., de la Rosa G., Parsons J.G., (2005). Phytoremediation of heavy metals and study of the metal coordination by X-ray absorption spectroscopy. *Coordination Chemistry Reviews* 249, 1797-1810.
- Gleba D., Borisjuk N.V., Borisjuk L.G., Kneer R., Poulev A., Skarzhinskaya M., Dushenkov S., Logendra S., Gleba Y.Y., Raskin I., (1999). Use of plant roots for phytoremediation and molecular farming. *Proceedings of the National Academy of Sciences of the United States of America* 96, 5973-5977.
- Kim J-W., Lee J-E., Ryu, J-H., Lee, J-S., Kim, S-J., Han, S-H., Chang, I-S., Kang, H-H, Suh, K-D., (2004). Synthesis of metal/polymer colloidal composites by the tailored deposition of silver onto porous polymer microspheres. *Journal of Polymer Science Part A: Polymer Chemistry* 42, 2551-2557.
- Lee H.J., S.Y. Yeo, Jeong, S.H., (2003). Antibacterial effect of nanosized silver colloidal solution on textile fabrics. *Journal of Materials Science* 38, 2199-2204.
- Lee J.H., Hossner L.R., Attrep M., Kung K.S., (2002). Uptake and translocation of plutonium in two plant species using hydronics. *Environmental Pollution* 117, 61-68.
- Lee P.C., Meisel D., (1982). Adsorption and surface-enhanced Raman of dyes on silver and gold sols. *Journal of Physical Chemistry* 86, 3391 – 3395.
- Lin D., Xing B., (2007). Phytotoxicity of nanoparticles: Inhibition of seed germination and root growth. *Environmental Pollution* 150, 243-250.
- Morones J.R., Elechiguerra J.L., Camacho, A., Holt, K., Kouri, J.B., Ramírez, J.T., Yacaman, M.J., (2005). The bactericidal effect of silver nanoparticles. *Nanotechnology* 16, 2346-2353.
- Pal S., Tak Y.K., Song M.J., (2007). Does the Antibacterial Activity of Silver Nanoparticles Depend on the Shape of the Nanoparticle? A Study of the Gram-Negative Bacterium *Escherichia coli*. *Applied and Environmental Microbiology* 73, 1712-1720.
- Pillai Z.S., Kamat P.V., (2004). What Factors Control the Size and Shape of Silver Nanoparticles in the Citrate Ion Reduction Method? *Journal of Physical Chemistry B* 108, 945 -951.

- Puebla R.A, Dos Santos Jr. D. S., Aroca R.F., (2004). Surface-enhanced Raman scattering for ultrasensitive chemical analysis of 1 and 2-naphthalenethiols. *The Analyst* 129, 1251-1256.
- Sileikaite A., Prosycevas I., Pulso J., Juraitis, A., Guobiene, A., (2006). Analysis of Silver Nanoparticles Produced by Chemical Reduction of Silver Salt Solution. *Materials Science* 12, 287-291.
- Sondi, I., Salopek-Sondi B., (2004). Silver nanoparticles as antimicrobial agent: a case study on E.coli as a model for Gram-negative bacteria. *Journal of Colloid and Interface Science* 275, 177-182.
- Toshikazu T., (1999). Antimicrobial agent composed of silica-gel with silver complex, *Inorganic Materials* 6, 505-511.
- Van der Schoot C., Aart J. E., (1989). Architecture of the Internodal Xylem of Tomato (*Solanum lycopersicum*) with Reference to Longitudinal and Lateral Transfer. *American Journal of Botany* 76, 487-503.
- Vigneshwaran N., Kathe A.A., Varadarajan, P.V., Nachane, R.P., Balasubramanya, R.H., (2006). Biomimetics of silver nanoparticles by white rot fungus, *Phaenerochaete chrysosporium*. *Colloids and Surfaces B: Biointerfaces* 53, 55-59.
- Yang L., Watts D.J., (2005). Particle surface characteristics may play an important role in phytotoxicity of alumina nanoparticles. *Toxicology Letters* 158, 122-132.
- Wang N., Zhang N., Wang M., (2006). Wireless sensors in agriculture and food industry – Recent development and future perspective. *Computers and Electronics in Agriculture* 50, 1-14.